A Dissertation on

OPTIMIZATION OF ENERGY GAIN IN THE BUBBLE REGIME OF LASER WAKEFIELD ACCELERATOR (LWFA)

Submitted in the partial fulfillment of the requirements of the degree of

MASTER OF TECHNOLOGY

In

NUCLEAR SCIENCE & ENGINEERING

By

RAM KRUSHNA MOHANTA

2K14/NSE/13

Under the Guidance of

Prof. S. C. Sharma

(Supervisor)

&

Dr. D. N. Gupta

(Joint-Supervisor)

Department of Applied Physics,

Delhi Technological University

(Formerly Delhi college of Engineering)

Govt. of NCT of Delhi

Main Bawana Road, Delhi-110042

YEAR: 2016

Department of Applied Physics

Delhi Technological University (DTU)

(Formerly Delhi College of Engineering, DCE)

Govt. of NCT of Delhi

Bawana Road, Delhi-110042

CERTIFICATE

*This is to certify that the Major project (AP-811) report entitled "***OPTIMIZATION OF ENERGY GAIN IN THE BUBBLE REGIME OF LASER WAKEFIELD ACCELERATOR (LWFA)***" is a bonafide work carried out by* **Mr. Ram Krushna Mohanta** *bearing Roll No.* **2K14/NSE/13**, *a student of Delhi Technological University, in partial fulfilment of the requirements for the award of Degree in* **Master of Technology** *in* "**Nuclear Science & Engineering**".

(**Prof. S. C. SHARMA**)
Supervisor
Head, Department of Applied Physics,
Delhi Technological University,
Delhi-110042

(**Dr. D. N. Gupta**)
Joint Supervisor
Assistant Professor,
Dept. of Physics & Astrophysics,
University of Delhi,
Delhi-110007

DECLARATION

I declare that this written submission represents my ideas in my own words and where others' ideas or words have been included, I have adequately cited and referenced the original sources. I also declare that I have adhered to all principles of academic honesty and integrity and have not misrepresented or fabricated or falsified any idea/data/fact/source in my submission. I understand that any violation of the above will be cause for disciplinary action by the Institute and can also evoke penal action from the sources which have thus not been properly cited or from whom proper permission has not been taken when needed.

PLACE:

DATE:

RAM KRUSHNA MOHANTA

(2K14/NSE/13)

ACKNOWLEDGEMENT

Every work accomplished is a pleasure- a sense of satisfaction. However a number of people always motivate, criticize and appreciate a work with their objective ideas and opinions, hence I'd like to thank all, who have directly or indirectly helped me accomplished this project.

Firstly I would like to thank my project supervisor Prof. S. C. Sharma without whose support this project could not be started in first place. Prof. Sharma, who took keen interest in my project, and guided me along until the completion of the project providing all necessary information.

Next I owe my profound gratitude to my co-supervisor Dr. D.N. Gupta for giving me an opportunity to do the project work in his lab and providing me all the support and guidance which made me complete the project in time. I am extremely thankful to Dr. Gupta for providing such a nice support and guidance even though he had a busy schedule managing university works and lectures.

I would also like to thank Ms. Maninder Kaur Panesar, Ph.D. scholar of University of Delhi, without whose assistance this project could not be completed. She has encouraged and guided me throughout the project explaining every tiny bit of detail and sacrificing time from her own schedule. It's been an extreme pleasure to work alongside her in the lab during the project.

Lastly, I would also like to mention Mr. Krishna Gopal, Ph.D. scholar of University of Delhi, who has been extremely helpful during difficulties in the project work and his contributions and inputs have been rather useful during simulation works. It's been really satisfying discussing the doubts and difficulties with him throughout the project.

I am also thankful to my other teachers, classmates and department staff for their constant support and encouragements.

Ram Krushna Mohanta

TABLE OF CONTENTS

	ABSTRACT	I
	LIST OF TABLES AND FIGURES	II
	LIST OF SYMBOLS	III
1.	INTRODUCTION	1-3
2.	LASER PLASMA INTERACTION	4-11
	2.1 Plasma	4
	2.2 Laser	6
	2.3 Non relativistic	9
	2.4 Relativistic	10
3.	LASER PLASMA ACCELERATORS	12-14
	3.1 PBWA	12
	3.2 SMLWFA	12
	3.3 LWFA	13
4.	CHARGED PARTICLE ACCELERATION	15-27
	4.1 Ponderomotive force	16
	4.2 Plasma wakefield generation	19
	4.3 Wave breaking	24
	4.4 Particle Trapping	25
5.	ACCELERATION IN BUBBLE REGIME	28-35
	5.1 Bubble regime	28
	5.2 Shape of the bubble	31
	5.3 Characteristics of bubble regime	32
	5.4 Particle trapping in the bubble	33
	5.5 Acceleration inside the bubble	34
6.	ACCELERATION LIMITS IN LWFA	36-39
	6.1 Laser Diffraction	36
	6.2 Pump depletion	36
	6.3 Electron Dephasing	37
	6.4 Laser plasma instabilities	39
7.	PARTICLE-IN-CELL METHOD	40-50
	7.1 Introduction	40
	7.2 Mathematical derivation	43

7.3 Advancing the particle 47
7.4 Algorithm 48
7.5 VORPAL Code 50
8. SIMULATION & RESULTS 51-63
8.1 Simulation Overview 51
8.2 Creating Input File 52
8.3 Optimization of Energy Gain 53
9. FUTURE PROSPECTS & APPLICATION 64-65
9.1 External Injection 64
9.2 Staging Acceleration 65
10. CONCLUSION 66
APPENDIX I
REFERENCES

ABSTRACT:

This work deals with optimization of the energy gain of the electrons inside the bubble in a LWFA. Acceleration of an electron to high energy in a short distance is now possible due to the development of laser Wakefield acceleration (LWFA). A compact-size high energy electron accelerator is possible with LWFA because the acceleration field in LWFA is 1000 times higher than that in the typical radio-frequency electron accelerator. The LWFA scheme also can generate an ultrashort electron bunch because the acceleration region in LWFA is very narrow. But the energy gain of electrons in a LWFA is limited by several factors, e.g. pump depletion, electron dephasing, and laser diffraction. To work around these limitation in LWFA requires increasing the laser plasma interaction length. So, in this work, a uniform density region followed by a ramp structure is employed as a plasma medium, through which laser propagates. Number of simulations have been conducted by varying the ramp length and keeping the laser parameters constant, and the effects were studied and simulation results were compared with each other. By varying the ramp length, variation in plasma channel density is achieved. As a result of variation in plasma density, the acceleration distance is directly affected, which in turns increases the energy gained by the electrons. The simulation results show that by employing upward density ramp, the energy gained by electrons have been increased from 100MeV to almost 300MeV. There is a significant increase in the bubble radius too, as the radius of the bubble increases the radial accelerating and focusing force have a dominant effect on the electron acceleration and the beam quality improves. Also with the increase in the density ramp length, the number of monoenergetic electrons getting trapped in the bubble increases. Another fact that is notice from this simulation is the bubble formation takes place in the uniform density region. And in the meantime the acceleration distance is also increased. As I am simulating the plasma with a 10 Tera-watt driver laser in non-linear regime ($a_0{}^2 \gg 1$), laser pump depletion limitation will be more evident than other factors. And the simulation shows that with increasing ramp length, the pump depletion length also increases. That means, the electrons are accelerated for more plasma length compared to one with uniform plasma density profile. All simulations are done in 2D-PIC codes with the help of VORPAL codes developed and marketed by Tech-X Corporation. The Vorpal outputs are, in the HDF5 format, analyzed using a python solver.

LIST OF TABLES

1. **Table 3.1**: Laser pulse length value for different types of pulses for maximum Wakefield
2. **Table 6.1**: Value of Acceleration length (L_{acc}) and energy gain (ΔW) in practical units for various Limitation factor

LIST OF FIGURES

1. **Fig.2.1 (Color):** Chirped Pulse amplification technique
2. **Fig.4.1 (Color):** (a) Plasma electrons are at equilibrium before LASER propagation (b) Plasma electrons are pushed from axial region due to Ponderomotive force after Laser Pulse
3. **Fig.4.2 (Color):** Plasma Wakefield Generation
4. **Fig.4.3:** Timed average Density perturbation (dashed curve) and axial electric field of Plasma Wake (Solid curve) in (a) Linear limit; (b) Non-linear limit;
5. **Fig.4.4 (color):** Plasma density perturbation excited by a Gaussian Laser pulse traveling a0 = 1.5
6. **Fig.4.5 (color):** Ocean wave analogy to Wave breaking phenomena
7. **Fig.4.6 (color):** Single electron orbits (dotted curves), separatrix (solid curve), and the dashed curve is the cold fluid orbit (dashed curve) (a) Shows an example of single electron orbits in ($\tilde{p}$, ξ) phase space (b) Shows acceleration of trapped electron in ($\tilde{p}$, ξ) phase space
8. **Fig 4.7 (color):** (a) Electron trapping. The upper dot represents an electron trapped within the dashed lines, the lower dot represents an untrapped electron which slips backward the wave. (b) Surfer (electron) trapped inside a rising ocean wave (Wakefield) as the wave converges (wave breaking) on itself.
9. **Fig.5.1 (color):** Shows the trapped electron inside a plasma bubble of nominal plasma density of 4×1025 m-3 driven by a laser of $A0$=4.0, laser Spot size of 8.5μm and the wavelength of the laser is 0.8μm
10. **Fig 5.2 (color):** The shape of the bubble at (a) 370μm (b) 570μm (c) 780μm (d) 950μm
11. **Fig 5.3:** Trajectory of trapped (solid line) and untrapped (dashed line) electron
12. **Fig.7.1 (color):** Point particle vs. Superparticles
13. **Fig.7.2:** Force contribution of point particle and superparticles respect to Debye length
14. **Fig 7.3:** First 3 b-spline functions
15. **Fig.7.4:** The Leap-frog algorithm
16. **Fig.8.1 (color):** Simulation Density structure

17. **Fig.8.2 (color):** Simulation 1 (Time step=1.26ps): Plasma Bubble formation at ~350μm at (a) Plasma density contour showing the bubble formation (b) Kinetic energy plot of plasma electron
18. **Fig.8.3 (color):** Simulation 1: (Time step=2.23ps) (a) Plasma density contour at maximum energy (b) Kinetic energy plot of plasma electrons at maximum energy position
19. **Fig.8.4:** Simulation 1: Histogram plot of plasma electrons at 2.23ps
20. **Fig.8.5 (color):** Simulation 1: Kinetic energy plot of plasma electrons during depletion at time step of (a) 2.76ps (b) 3.5ps (c) Laser electric field plot at 1.26ps (d) Laser field plot at 2.76ps
21. **Fig.8.6 (color):** Simulation 2 (Time step=1.71ps): (a) Plasma density contour during bubble formation (b) Kinetic energy plot of plasma electrons
22. **Fig 8.7 (color):** Simulation 2 (Time step=2.6ps): (a) Plasma density contour at maximum energy (b) Kinetic energy plot of plasma electrons
23. **Fig.8.8:** Simulation 2: Histogram plot of plasma electrons at 2.6ps
24. **Fig.8.9 (color):** Simulation 2: Laser electric field plot at (a) Formation of bubble time step=1.71ps (b) depletion of laser Time step=3.11ps
25. **Fig.8.10 (color):** Simulation 3: (Time step=2.15ps) (a) Plasma bubble forms at ~600μm (b) Kinetic Energy plot of plasma electrons
26. **Fig.8.11 (color):** Simulation 3: (Tim step=3.27 ps): (a) Plasma density contour at maximum energy (b) Kinetic energy plot of plasma electrons at Maximum energy
27. **Fig.8.12 (color):** Simulation 3: Histogram plot of plasma electrons at 2.6pS
28. **Fig.8.13 (color):** Simulation 3: Laser electric field (a) 2.15 ps (b) 3.27 ps
29. **Fig.8.14 (color):** Simulation 4: (Time step=2.5ps) (a) Plasma bubble formation at 720μm (b) Kinetic Energy plots of Plasma electrons at bubble formation
30. **Fig 8.15 (color):** Simulation 4: (Time step=3.6 ps) (a) Plasma density contour at maximum energy position (b) Kinetic energy Plot of plasma electrons at Maximum energy
31. **Fig 8.16 (color):** Simulation 4: (a) Kinetic energy plot of plasma electrons shows Secondary injection takes place at Time step=3.8 ps and first injection energy spread and peak starts to decrease. (b) Histogram plot of plasma electron at 3.6ps
32. **Fig.8.17 (color):** Simulation 4: Laser electric field plot at (a) Time step= 2.5 ps (b) Time step=4.56 ps
33. **Fig.9.1 (color):** A two-staged laser plasma accelerator

LIST OF SYMBOLS AND CONSTANTS

$\hbar = Planck's\ constant = 6.62607004 \times 10^{-34}\ \mathrm{m^2.\ kg.\ s^{-1}}$

$\omega_p = Electron\ Plasma\ Frequency$

$n_o = Equllibrium\ electron\ plasma\ density$

$e = charge\ of\ the\ electron = 1.60217662 \times 10^{-19}$ coulombs

$\varepsilon_0 = permitivity\ in\ free\ space = 8.85418782 \times 10^{-12}\ \mathrm{m^{-3}\ kg^{-1}\ s^4\ A^2}$

$\mu_0 = permiability\ in\ free\ space = 4\pi \times 10^{-7}\ kg.m.s^{-2}.A^{-1}$

$m = rest\ mass\ of\ electron = 9.10938356 \times 10^{-31}\mathrm{kg}$

$\lambda_D = Debye\ length$

$K = Boltzman's constant = 1.38064852 \times 10 - 23\ \mathrm{m^2\ kg\ s^{-2}\ K^{-1}}$

$N_D = Number\ of\ particles\ per\ unit\ volume$

$\tau = Laser\ pulse\ duration$

$v = frequency\ of\ incident\ photon\ (Hz)$

$\vec{A} = Vector\ potential$

$\emptyset = Electrostatic\ scalar\ potential$

$\vec{B} = Magnetic\ field$

$\vec{E} = electric\ field$

$\rho = charge\ density$

$\vec{J} = current\ density$

$\vec{v}_q =\ quiver\ velocity$

$\vec{P} = Pressure\ gradient\ force$

$c = speed\ of\ light = 3 \times 10^8\ {}^{m}/_{s}$

$\lambda = wavelength\ of\ the\ laser\ (m)$

$r_0 = laser\ spot\ size$

$L = laser\ pulse\ length$

$k = laser\ propagation\ vector = \frac{2\pi}{\lambda}$

$\omega = laser\ frequency\ in\ vaccum = ck$

$a_0 = laser\ strength\ parameter$

$I_0 = Peak\ laser\ intensity$

$P = power\ of\ laser$

$v_g = Laser\ Group\ velocity$

$v_{ph} = Laser\ Phase\ velocity$

$\eta = plasma\ refractive\ index$

$\gamma = lorentz\ factor = \frac{1}{\sqrt{1 - {v^2}/{c^2}}}$

CHAPTER I

1. INTRODUCTION

Man has devoted a large part of scientific researches and resources to know the creation of the world. He has built various devices to search for the answers; Particle Accelerators. As the name suggests, a particle accelerator simply accelerate a particle, in this case they are sub atomic. Now the question arises, why accelerate a sub atomic particle? As De-Broglie has suggested the wavelength of the probe should be smaller than the size of the object to be probed. De-Broglie's wavelength:$\lambda = \frac{\hbar}{\sqrt{2mE}}$, so to probe matters on smaller scale, we need particle with higher energy, and thus comes the usage of Particle accelerator. Particle Accelerators have been developed since early 20th century and numerous types of accelerators have been developed, like LINACS, Cyclotron, Pelletron, Synchrotron and Betatron. But all these accelerators have been limited by one factor the dielectric breakdown of the medium. So the particle can be accelerated only up to few Hundred MeV. But as the need for higher energy particles increases, in 1956, Vekslar proposed a method to accelerate the particle in a plasma medium by an electron beam driver. In 1960 T. Mainman invented LASER. But, the intensity of laser was not high enough to drive a plasma medium. But prior to 1970, as the laser technology grows in strength and power and able to deliver high intensity laser, in 1979 Tajima and Dawson [1] proposed use of laser beam to excite plasma wave to accelerate electron; Laser Wakefield Acceleration (LWFA) Technique. And thus starts the era of Laser Plasma Accelerators, those could accelerate any particles up to thousands of GeV and produces a much better resolution of output beam than the conventional accelerators'.

Even the Laser plasma Accelerators have their own limitation which hinders the energy gain, and in this work I have worked to optimize the energy gain of a LWFA for different types of density profile of plasma. As the plasma accelerators are driven by high intensity laser and the plasma density are of the order of 10^{25} m^{-3} the interaction between laser and plasma falls in relativistic region. So the Maxwell's equation which describes the electromagnetic field of a plasma becomes very difficult to solve analytically, and numerical methods have to be

approached. Even the numerical solution poses serious number of calculation and takes terabytes of memory and requires fast processors. Another difficulty was, in previous calculations plasma was treated as fluid, in which the information regarding specific movements of particles were lost due to consideration of macroscopic value. So a new technique Particle-In-Cell (PIC) was developed by Buneman (1959) [2] to solve these problems. This technique solves a plasma density of the order of 10^{25} particles by simulating only 10^{9} or 10^{12}particles. So it saves lots of computational costs and time as well. As this method has been refined and developed over time, now we can study any laser plasma interactions and behavior of the Wakefield, various plasma properties and output beam by simulations. Now the computational time has been further reduced and 3-dimensional view of simulations can be developed using cluster or networked CPUs which performs the simulations in parallel.

In this work, I have used a software VORPAL 5.2.6 developed by Tech-X [3] corporation to study and optimize the energy gain of the electron in LWFA. VORPAL is used for modeling plasma thrusters, vacuum electronics, photonic devices, Laser Wakefield Accelerator, fusion plasmas and multipactor effects in Superconducting RF cavities. Originally developed by the Plasma and Beam Physics Group at the University of Colorado, VORPAL is currently developed and marketed by Tech-X Corporation. It has a flexible architecture that helps it to run 1D, 2D as well as 3D simulations depending on the cluster and memory available. The plasma in VORPAL can be simulated as fluid and kinetic model depending upon the user's choice. VORPAL gives the output data in HDF5 (Hierarchical Data Format) and can be extracted through any visualization tools such as MATLAB and VisIt. But here I have used a python script to extract and analyze the data.

This article has been divided into number of sections for reader's convenience. A brief overview on plasma, laser and their interaction mechanism has been given in Chapter II. Chapter III describes the various types of Laser Plasma Accelerators in use, and as our work is based on LWFA, more emphasis has been given on so. In Chapter IV, the whole mechanism of Ponderomotive force, Wakefield generation, wave breaking and trapping in a LWFA has been discussed. Chapter V describes the particle acceleration in bubble regime of LWFA. And an overview of the factors affecting maximum energy gain are given in Chapter VI. The detail

technique of Particle-In-Cell (PIC) is discussed in Chapter VII. Simulations and results are given in Chapter VIII.

Before we divulge into the topic, I want to remind the readers that all the expressions and constants are in S.I. units unless stated otherwise. As Fluid dynamics concepts are insufficient to describe the kinetic effects and hence kinetic model has been used.

CHAPTER II

2. LASER PLASMA INTERACTION

2.1 PLASMA

Although this work is based on advanced plasma physics topics, it is necessary to define the basic plasma parameters in the beginning to have a better understanding of the physics. By basic definition Plasma can be said as the fourth state of matter, but if we want a technical definition that gives us a better idea about what is plasma, the perfect definition of plasma; "*Plasma is a quasi-neutral gas of charged and neutral particles which exhibits collective behavior."* This definition separates plasma from any ionized gas.

By quasi-neutral we mean that the plasma is neutral enough to consider $n_i \approx n_e = n_0$, where n_i is the ion density and n_e is the electron density which is equal to the equilibrium plasma density n_0, but not enough so that all the electromagnetic forces vanishes.

Another property of plasma is the collective behavior. By saying collective behavior we states that the macroscopic result of any external field will be a cooperative response of all plasma particles. A macroscopic force applied to a neutral gas is transmitted to the individual atoms by collisions due to the absence of any electromagnetic forces and negligible gravity. The situation is totally different in plasma, which has charged particles. As these charges move around, they can generate local concentrations of positive or negative charge, which give rise to electric fields. Motion of charges also generates currents, and hence magnetic fields. These fields affect the motion of other charged particles far away.

Now let's define some basic plasma properties which will be used in further chapters.

Electron plasma frequency $(\omega_p) = \sqrt{\frac{n_o e^2}{\varepsilon_0 m}}$, ... (2.1)

where $n_o (\approx n_e) = electron\ plasma\ density$

$e = charge\ of\ the\ electron = 1.60217662 \times 10^{-19}$ coulombs

$\varepsilon_0 = permitivity\ in\ free\ space = 8.85418782 \times 10^{-12}\ \mathrm{m^{-3}\ kg^{-1}\ s^4\ A^2}$

$m = rest\ mass\ of\ electron = 9.10938356 \times 10^{-31}\mathrm{kg}$

In our work, we have only considered electron plasma frequency because of negligible ion motion.

$$\text{Debye length } (\lambda_D) = \sqrt{\frac{\varepsilon_0 K T_e}{ne^2}} \quad \ldots (2.2)$$

Debye length is defined as the length up to which plasma can shield any potential. Debye length can also be used to define number of particles per unit volume

$$N_D = \frac{4}{3}\pi n {\lambda_D}^3 \quad \ldots (2.3)$$

In general any ionized gas to be defined as plasma must satisfy 3 conditions

1. $\lambda_D \ll L$ ... (2.4)
2. $N_D \gg 1$ ... (2.5)
3. $\omega\tau \gg 1; Avg.no\ of\ collision$ ... (2.6)

The dynamics of plasma is defined by four Maxwell's equation, Equation of motion and the equation of continuity. All Maxwell's equations presented below are in differential form and S.I. unit.

1. Maxwell's 1st equation also known as Gauss's law of electricity.

"*Electric flux out of any closed surface is equal to total charge enclosed within the surface."*

$$\nabla . \vec{B} = \frac{\rho}{\varepsilon_0} \quad \ldots (2.7)$$

2. Maxwell's 2nd equation also known as gauss's law of magnetism.

"Magnetic flux out of any closed surface is zero"

$$\nabla . \vec{B} = 0 \quad \ldots (2.8)$$

3. Maxwell's 3rd equation; Faraday's law of induction

"The voltage accumulated around a closed circuit is proportional to the time rate of change of the magnetic flux it encloses."

$$\vec{\nabla} \times \vec{E} = -\frac{\partial \vec{B}}{\partial t} \quad \ldots (2.9)$$

4. Maxwell's 4th equation; Ampere's Law

"Electric currents and charges in electric fields are proportional to the magnetic field circulating about the area they pierce."

$$\vec{\nabla} \times \vec{B} = \mu_0 \left(\vec{J} + \varepsilon_0 \frac{\partial \vec{E}}{\partial t} \right) \quad \ldots (2.10)$$

Now the two most important equation that defines plasma parameters in a kinetic model are equation of motion and equation of continuity.

5. Equation of motion:

$$\vec{F} = m\frac{d\vec{v}}{dt} = -e\vec{E} - e\left(\vec{v} \times \vec{B}\right) - \frac{\nabla\vec{P}}{n} - m\vec{\vartheta}v\,, \qquad \ldots(2.11)$$

where $-e\vec{E} = force\ due\ to\ the\ electric\ field.$

$-e\left(\vec{v} \times \vec{B}\right) = force\ due\ to\ the\ magnetic\ field.$

$-\frac{\nabla\vec{P}}{n} = pressure\ grsdient\ force.$

$-m\vec{\vartheta}v = force\ due\ to\ the\ collision.$

In this work, the pressure gradient force and collisional force are neglected in most of the cases, unless stated otherwise.

6. Equation of Continuity:

$$\frac{\partial\rho}{\partial t} + \nabla.\vec{J} = 0\,, \qquad \ldots(2.12)$$

where $\rho = charge\ density\ and\ \vec{J}\ is\ the\ curent\ density = -ne\vec{v}$, which can further be represented as below:

$$\frac{\partial n}{\partial t} + \nabla.(\mathrm{n}\vec{v}) = 0 \qquad \ldots(2.13)$$

2.2 LASER

The evolution of laser dates back to 1917, when Einstein proposed a theory of "stimulated emission" that makes the LASER possible. The theory of stimulated emission states that a bunch of excited electrons can be interacted with an incoming photon of certain frequency in such a manner that the interaction process emits a light of particular wavelength. The whole process can be described by the expression below:

$$E_2 - E_1 = hv\,, \qquad \ldots(2.14)$$

where $E_2 = Energy\ of\ excited\ state\ electron$s

$E_1 = Energy\ of\ ground\ state\ electrons$

$h = Planck's\ constant = 6.626176 \text{ x } 10^{-34}$ joule $-$ seconds

$v = frequency\ of\ incident\ photon\ (Hz)$

But it took 40 years for the LASER to be intensified to such a level that it could be efficiently used in a Laser plasma interaction process. Today, the laser power ranges from milli-Watt Laser pointers to High power CO_2 Laser having power ranges around 3000 Mega-Watt. The most powerful laser is at Osaka University in Japan, where the Laser for Fast Ignition Experiments (LFEX) has been boosted to produce a beam with a peak power of two peta-watts in picosecond range.

For efficient laser plasma interaction processes, the laser needs to be of High Intensity and non-linear in nature (Laser strength parameter $a_0^2 >> 1$) with incredible short duration, desirably in pico-second or femto-second range. Although laser in linear regime ($a_0^2 << 1$) can also be used but the effect would not be as significant and visible as in former case. To produce such a laser, Chirped-pulse amplification technique is used, where the laser is first stretched in time and then amplified and then recompressed.

Fig.2.1 (color): Chirped Pulse amplification technique

An important parameter in discussion in laser plasma interaction is the laser strength parameter a_0 defined as the peak amplitude of the normalized vector potential of a laser field. The laser strength parameter is related to peak laser intensity (I_0) and Power (P) defined by the below expression.

$$I_0 = \left(\frac{\pi c}{2}\right)\left(\frac{mc^2 a_0}{e\lambda}\right)^2 \quad \ldots (2.15)$$

$$P = \frac{\pi {r_0}^2 I_0}{2} \quad \ldots (2.16)$$

which yields the expression $a_0 = 7.3 \times 10^{-19}[\lambda(\mu m)]^2 I_0 \left(\frac{W}{cm^2}\right)$ ... (2.17)

Where a linearly polarized Gaussian laser profile is assumed

$$\vec{a} = a_0 \exp\left(\frac{-r^2}{{r_0}^2}\right)\cos(kz - \omega t)\,.\,\hat{z} \quad \ldots (2.18)$$

where $\vec{a} = normalized\ vector\ potential\ of\ laser\ field$

$m = mass\ of\ electron = 9.1 \times 10^{-31}\ kg$

$c = speed\ of\ light = 3 \times 10^8\ {}^{m}/_{S}$

$e = charge\ of\ electron = 1.6 \times 10^{-19}\ coloumb$

$\lambda = wavelength\ of\ the\ laser\ (m)$

$r_0 = laser\ spot\ size$

$k = laser\ propagation\ wave\ vector = \frac{2\pi}{\lambda}$

$\omega = laser\ frequency\ in\ vaccum = ck$

If not otherwise stated, such a pulse is used in all further calculation as well as simulations.

The plasma target involved in such an interaction of high intensity laser beam is automatically becomes relativistic in nature. Due to the very high intensity of ultra-short laser pulse the plasma electron velocity reaches close to the velocity of light. After achieving relativistic velocities the electrons may exhibit collective behavior, which give rise to very high amplitude electron plasma wave, called Wake field effect, which we would discuss in later chapter.

2.3 NON-RELATIVISTIC INTERACTION

In non-relativistic interaction the laser travels with a velocity less than the light velocity. For the propagation of such a laser pulse inside plasma, the plasma dispersion relation can provide lot of information.

The dispersion relation of plasma is

$$\omega^2 = {\omega_p}^2 + c^2k^2 \ , \qquad \ldots(2.19)$$

where $\omega = angular\ frquency\ of\ laser\ pulse$ and $\omega_p = electron\ plasma\ frquency$

As the laser pulse is relativistic in nature and traveling at a lesser velocity than c, the pulse has group velocity of v_g and phase velocity of v_{ph}, and it holds that

$$\frac{c}{v_g} = \frac{v_{ph}}{c}$$

$$\text{which yields,} \quad c^2 = v_{ph}v_g \qquad \ldots(2.20)$$

The phase velocity of laser propagating in vacuum is $v_{ph}(= \frac{\omega}{k})$ $\ldots(2.21)$

By combining equation (2.20) and (2.21) and putting it into equation (2.19), the phase velocity for the laser is found to be

$$v_{ph} = \frac{c}{\sqrt{1 - \frac{{\omega_p}^2}{\omega^2}}} \qquad \ldots(2.22)$$

which gives the expression for refractive index of plasma in relativistic region

$$\eta = \frac{c}{v_{ph}} = \sqrt{1 - \frac{{\omega_p}^2}{\omega^2}} \qquad \ldots(2.23)$$

As the equation (2.23) suggests, for laser with $\omega < \omega_p$, the refractive index η becomes imaginary, and the laser will reflect back. So only a laser having frequency more than electron plasma frequency can travel through that plasma.

For a certain laser frequency, $\omega = \omega_p$, and the density at that electron plasma frequency is called critical density given by

$$n_{critical} = \frac{\omega^2 \varepsilon_0 m}{e^2} \quad \ldots (2.24)$$

2.4 RELATIVISTIC INTERACTION

Since this work deals with Laser Wakefield accelerator driven by high intensity laser, we have to assume relativistic case of plasma. In case of relativistic interaction, the laser is travelling with a phase velocity close to the velocity of light, so the refractive index of plasma will change to

$$\eta_{relativistic} = \sqrt{1 - \frac{{\omega_p}^2}{\gamma \omega^2}} \quad \ldots (2.25)$$

Because the relativistic electron plasma frequency will change to ${\omega_{p(relativistic)}}^2 = \frac{{\omega_p}^2}{\gamma}$

And the relativistic electron plasma density is

$$n_{relativistic} = \frac{{\omega_{p(relativistic)}}^2 \varepsilon_0 m}{e^2} = \frac{{\omega_p}^2 \varepsilon_0 m}{\gamma e^2} \quad \ldots (2.26)$$

NOTE: “m” is considered as the rest mass of electron unless stated otherwise.

Combining equation (2.24) and (2.26), the relativistic refractive index can be written as

$$\eta_{relativistic} = \sqrt{1 - \frac{n_o}{\gamma\, n_{critical}}} \quad \ldots (2.27)$$

where $\gamma = relativistic\ gamma\ factor = \frac{1}{\sqrt{1 - {v^2}/{c^2}}}$

So the increase in refractive index acts likes a collecting lens and acts against the usual defocusing of a laser pulse behind its focus. So with the correct relativistic plasma frequency,

which ultimately depends on electron plasma density, one can send a laser pulse over long distances through plasma without suffering from defocusing.

This is another benefit of using a relativistic laser; it creates a self-focusing effect [4], which assists the laser to travel a long distance in plasma, thus increasing the laser plasma interaction length. To take full advantage of this self-focusing effect Sprangel et al, (1987) [5] showed that the laser pulse length L must be less than plasma wavelength λ_p.

Such High intensity lasers create novel states of matter; for instance, electrons oscillate at relativistic velocities, which results in relativistic mass changes exceeding the electron rest mass. At this point, the magnetic field of the electromagnetic wave also becomes important. Electrons behave in such fields as if the light wave was rectified. The propagation of light also depends in this regime on the light intensity, resulting in nonlinear effects. Thus, a new field of nonlinear optics, which of relativistic electrons, has opened up. Rapid advancement in our understanding is underway and new research tools, subfields and commercial products are on the horizon, like compact and ultra-short pulse duration *laser-based electron accelerators* [6].

As there are new advances in the field of producing ultrafast very high intensity laser, it has opened up the field of the application of laser plasma interaction; few of them are; Black Hole Study, Ion propulsion, Proton Therapy, Ultra-fast imaging technique, Fast igniter fusion, Free Electron Laser application, *Laser-Driven Plasma Accelerator*.

But In this work, we mainly concentrate on the Laser Driven Plasma Acceleration technique as most of our work is related to charge particle acceleration, where we use the theory of laser plasma interaction to obtain and optimize the maximum energy gain of an electron in a laser driven plasma accelerator.

Now to clarify a sensible question that, why use plasma as an accelerating medium? Why this cannot be done in vacuum or gas? Vacuum and Gaseous medium suffers from breakdown and ionization limitation. But plasma can be fully preionized, so there is no such limitation. Diffraction can be overcome through self-focusing and with preformed plasma channels.

Plasma medium acts as a “Transformer”, converting the transverse laser field into the axial electric field of plasma wave. This is not possible in case of vacuum or gaseous medium.

Another advantage of using plasma as an accelerating medium is self-injection [7] of electron from plasma medium.

CHAPTER III

3. LASER PLASMA ACCELERATORS

There are few different types of laser plasma acceleration technique, those employs different methods for electron acceleration.

3.1 PLASMA BEAT WAVE ACCELERATOR

The PBWA technique was first proposed by Tajima and Dawson in (1979) [1] as an alternative to LWFA since ultra-short and high power laser was not available at that time. In this LPA, two Long LASER pulses of different frequencies are beat together to create a Plasma Wakefield. This is done by appropriately adjusting the laser frequencies and plasma density to satisfy resonant condition $\Delta\omega = \omega_1 - \omega_2 = \omega_p$. Consider two laser pulses combined with normalized vector potentials given by

$$a = a_{01}\cos(k_1 z - \omega t) + a_{02}\cos(k_2 z - \omega t) \quad \ldots (3.1)$$

Both laser pulses must satisfy resonant condition to generate the maximal Wakefield. The PBWA suffers from a limitation called “resonant detuning” [8]. As the plasma wave amplitude increases, the plasma wave period increases. Since the period of beat wave is fixed, the plasma wave eventually gets out of phase with laser beat wave. To overcome this problem, laser pulses are chirped to compensate for change in non-linear plasma wavelength, resulting in a significant increase in plasma wave amplitude. Another method of auto-resonant phase locking of plasma wave to the slowly chirped beat frequency of lasers also been proposed. In addition to resonant detuning, PBWA suffers from common laser plasma instabilities too due to the fact that it uses long laser pulses.

3.2 SELF MODULATED LASER WAKEFIELD ACCELERATOR

Self-Modulated LWFA is a hybrid scheme combining elements of stimulated Raman forward scattering (RFS) [9] and the laser Wakefield concept. Under certain conditions, it is possible for a single long laser pulse to break up into a train of short pulses, each of these short pulses having a width on the order of plasma wavelength. Now this pulse train creates large amplitude plasma

wave. This process is referred to as self-modulation. To operate in self-modulation regime, the pulse length has to be large compared to plasma wavelength ($L > \lambda_p$) and pulse power must be greater than power required to guide a long laser pulse ($P > P_c$).

The advantage of SLWFA is that

(a) It operates at high density, so higher plasma wakefield will be generated ($E \propto \sqrt{n_0}$)

(b) The higher laser pulse intensity has higher a_0, so it increases the plasma Wakefield as well.

(c) The wakefield is resonantly excited, i.e. excited by a series of small beam rather than single one as in LWFA

(d) Relativistic optical guiding allows the modulate pulse to propagate through several Rayleigh lengths, thus increases the accelerating length.

Disadvantages of SLWFA:

(a) At higher density the laser pulse group velocity decreases, the electron dephase from Wakefield phase so it limits the accelerating distance.

(b) The energy spread of output beam is broad due to continual trapping and short dephasing length.

(c) Diffraction of modulated pulse structure

3.3 LASER WAKEFIELD ACCELERATOR

LWFA was first proposed by Tajima & Dawson (1979) [1]. But as the technology to produce a high intensity short laser pulse was not developed at that time, PBWA seemed feasible at that time. But after 1985 the technology to generate ultra-intense picosecond laser pulse has been developed and LWFA was reinvented. LWFA offers longitudinal accelerating fields of the order of 100 GV/m, many orders of magnitude larger than conventional accelerators and it enables the generation of few-fs pulse duration electron bunches. In LWFA a very high intensity short laser pulse was passed through an underdense plasma, the ponderomotive force associated with the pulse ($F_p \propto \nabla a^2$), where a is the normalized vector potential of laser electric field, expels the electron from high pressure region to low pressure region, thus creating an electron deprived region in the axis region. And this effect produces a high gradient plasma Wakefield which is used to accelerate particles. To generate maximum Wakefield the laser pulse length must be in

the order of plasma wavelength ($L \propto \lambda_p$). Below are some values for optimum pulse length condition for maximum plasma Wakefield.

In this work, all our simulations are based on LWFA techniques and Laser pulse is linearly polarized Gaussian pulse of the form $a = a_0 \exp\left(\frac{-r^2}{{r_0}^2}\right) \cos(kz - \omega t)\, \hat{z}$ which can be further represented in a co-moving frame of reference as below:

$$a = a_0 \exp\left(\frac{-\xi^2}{4{L_{rms}}^2}\right) \cos(k\xi) \qquad \ldots (3.2)$$

TABLE 3.1[10]

LASER PULSE TYPE	Root Mean Square Length ($k_p L_{rms}$)	Full width at half maximum length (L_{FWHM})	Maximum Wakefield Amplitude ($E_{\max}$)
Square	0.91	$0.5\lambda_p$	${a_0}^2 E_0$
Sine	0.95	$0.42\lambda_p$	$0.82{a_0}^2 E_0$
Gaussian	1.0	$0.37\lambda_p$	$0.76{a_0}^2 E_0$

Advantages of LWFA:

1. Because the plasma wave is driven by a single laser pulse with $L \sim \lambda_p$, the Wakefield amplitude is relatively insensitive to uncertainties in the pulse duration and the Plasma uniformity.
2. Furthermore, since the laser pulse in the LWFA is of short duration $L \sim \lambda_p$, various instabilities that can be detrimental to the propagation of long pulses can be reduced.

However even LWFA also suffers from some limitation like pump depletion, laser diffraction, electron dephasing, laser plasma instabilities like stimulated forward and backward Raman scattering which tend to limit the energy gain of the output beam in LWFA.

In this work, our main concentration is to enhance the energy gain by optimizing the electron dephasing limit through different types of plasma density profile through PIC simulation. So our main focus will be on the single LWFA limitation i.e., electron dephasing which will be discussed in detail in further chapters

CHAPTER IV

4. CHARGE PARTICLE ACCELERATION

Laser driven plasma accelerator are growing interest as there is advancement in producing High intensity laser pulse which can be used to ionize plasma to accelerate electron and can produce much more energized particle than conventional RF accelerator. The RF accelerators are limited by the dielectric breakdown field limit, typically of the order of 20-50MeV/m whereas plasma based accelerator can sustain up to 200GeV/m. Also the structure and facility used in conventional acceleration technique is too large compared to plasma acceleration technique where much faster and better resolution beam can be obtained even at milli-meter length.

$$E_0(V/m) = \frac{cm_e\omega_p}{e} \approx 96\sqrt{n_0(cm^{-3})} \quad \ldots (4.1)$$

where $\omega_p = electron\ plasma\ frequency$

$n_0 = elceron\ density$

Equation 4.1 is the cold non relativistic wave breaking limit [11]. As the above expression suggests, a plasma having a density of 10^{18} cm^{-3} can yield a field ~100 GeV/m. To achieve this type of electric gradient in a RF Linacs more than 5 km long structure is needed.

Another advantage of Plasma based accelerator is that they have a tendency to produce extremely short electron bunches. The length of accelerating wave in LPAs is approximately equal to the plasma wavelength (λ_p).

$$\lambda_p \approx \frac{3.3 \times 10^{10}}{\sqrt{n_0(cm^{-3})}} \quad \ldots (4.2)$$

To produce maximum energy gain value for the particle, the plasma wavelength must be of the order of laser pulse length, this enables a wide variety of pump-probe application.

Another condition for the laser to be satisfied in LPA is that $\lambda_p \gg \lambda$.

As the dispersion relation for plasma suggests $\omega^2 = {\omega_p}^2 + k^2c^2$ ... (4.3)

If $laser\ frequency\ (\omega) < electron\ plasma\ frequency\ (\omega_p)$, propagation vector (k) is Imaginary. Wave will reflect back, and no Wakefield generation will take place. On the other hand if $laser\ frequency\ (\omega) > electron\ plasma\ frequency\ (\omega_p)$, propagation vector (k) is real and the laser pulse will propagate through plasma medium.

4.1 PONDEROMOTIVE FORCE

"*Ponderomotive force* [12] *is the non-linear force that a charged particle experience in an inhomogeneous electromagnetic field."*

It can be derived from the electron fluid equation of motion in cold fluid limit.

Electron fluid equation of motion: $m\frac{d\vec{v}}{dt} = -e\left[\vec{E} + \vec{v} \times \vec{B}\right]$ ... (4.4)

Electron fluid momentum equation: $\frac{d\vec{p}}{dt} = -e\left[\vec{E} + \vec{v} \times \vec{B}\right]$, ... (4.5)

where $\vec{p}\&\vec{v}\ are\ plasma\ fluid\ element\ momentum\ and\ velocity, respectively.$

The Electric field $(\vec{E})$ and Magnetic field $(\vec{B})$ of the laser can be written as follows:

$$\vec{E} = -\frac{\partial \vec{A}}{\partial t} \quad \text{... (4.6)}$$

$$\vec{B} = \vec{\nabla} \times \vec{A}, \quad \text{... (4.7)}$$

where $\vec{A}\ is\ the\ Laser\ vector\ potential\ and\ \vec{A} = A_0 \exp\left(\frac{-r^2}{{r_0}^2}\right)\cos(kz - \omega t)\,\hat{z}$

In the linear limit, $|a| = \frac{e|A|}{mc^2} \ll 1$.

The direction of vector potential of laser is in the transverse direction, which in our case is in Z-polarized (perpendicular to direction of motion) same in the direction of electric field.

Now due to the High electric field of Laser, the electrons in plasma will quiver at a velocity $\vec{v}_q, called$ quiver velocity and the momentum associated with it is called quiver momentum $\vec{p}_q$. Considering that the perturbation caused by the wave is small - that is to

say$\vec{A}$ is a first-order term - and that the frequency is high enough to neglect the motion of the ions, we can linearize the collisionless electron momentum equation into

$$m\frac{d\vec{v}_q}{dt} = -e\vec{E} = e\frac{\partial \vec{A}}{\partial t} \quad \ldots (4.8)$$

$$\vec{v}_q = \frac{e}{m}\vec{A} \quad \ldots (4.9)$$

Now the total velocity can be written as $\vec{v} = \vec{v}_q + \overrightarrow{\delta v}$, ... (4.10)

The quiver velocity $\vec{v}_q$ is the first order velocity and $\overrightarrow{\delta v}$ is the perturbation in velocity due to laser. We are ignoring all higher order velocity contribution. Now we have to derive the force causing the velocity perturbation, which will be our Ponderomotive force.

Differentiating the Equation (4.10) w.r.t time (t) and multiplying with electron mass (m), we obtain,

$$m\frac{d\vec{v}}{dt} = m\frac{d\vec{v}_q}{dt} + m\frac{d\overrightarrow{\delta v}}{dt} \quad \ldots (4.11)$$

Using in the value from equation (4.4) and equation (4.10) in equation (4.11)

$$\left[-e\vec{E} - e(\vec{v}\times\vec{B})\right] = m\left(\frac{\partial \vec{v}_q}{\partial t} + \left(\vec{v}_q.\nabla\right)\vec{v}_q\right) + m.\frac{d\overrightarrow{\delta v}}{dt} \quad \ldots (4.12)$$

Now putting the value of $\vec{E}$ & $\vec{B}$ in terms of vector potential we get,

$$e\frac{\partial \vec{A}}{\partial t} - e\left(\vec{v}_q \times \left(\vec{\nabla}\times\vec{A}\right)\right) = m\frac{\partial \vec{v}_q}{\partial t} + m\vec{v}_q(\vec{v}_q.\nabla) + m\frac{d\overrightarrow{\delta v}}{dt}$$

$$-e\left(\vec{v}_q \times \left(\vec{\nabla}\times\vec{A}\right)\right) = m\vec{v}_q\left(\vec{v}_q.\nabla\right) + m\frac{d\overrightarrow{\delta v}}{dt}$$

$$m.\frac{d\overrightarrow{\delta v}}{dt} = -e\left(\vec{v}_q \times \left(\vec{\nabla}\times\vec{A}\right)\right) - m\vec{v}_q\left(\vec{v}_q.\nabla\right) \quad \ldots (4.13)$$

Using the value of $\vec{v}_q$from equation (4.9), we get

$$m.\frac{d\overrightarrow{\delta v}}{dt} = \frac{-e^2}{m}\left[\vec{A}\times\left(\vec{\nabla}\times\vec{A}\right) + \vec{A}.\left(\nabla.\vec{A}\right)\right] \quad \ldots (4.14)$$

Now using the vector identity $\vec{\nabla}.F^2 = \vec{\nabla}(\vec{F}.\vec{F}) = 2\vec{F} \times (\vec{\nabla} \times \vec{F}) + 2\vec{F}(\vec{\nabla}.\vec{F})$ in equation (4.14), we get:

$$m.\frac{d\vec{\delta v}}{dt} = \frac{-e^2}{2m}.\vec{\nabla}A^2 = F_p \qquad \ldots(4.15)$$

This is the expression for the Ponderomotive Force. If a region in space, the electric field has non-uniform amplitude, Ponderomotive force compels the electron to go from High pressure region to low pressure region.

$$F_p = \frac{-e^2}{2m}.\vec{\nabla}|A|^2 = \frac{-e^2}{4m\omega^2}.\vec{\nabla}|E|^2 \qquad \ldots(4.16)$$

Where $|A| = \frac{|E|}{2\omega}$.

This is the ponderomotive force in 3D-linear regime (${a_0}^2 \ll 1$).

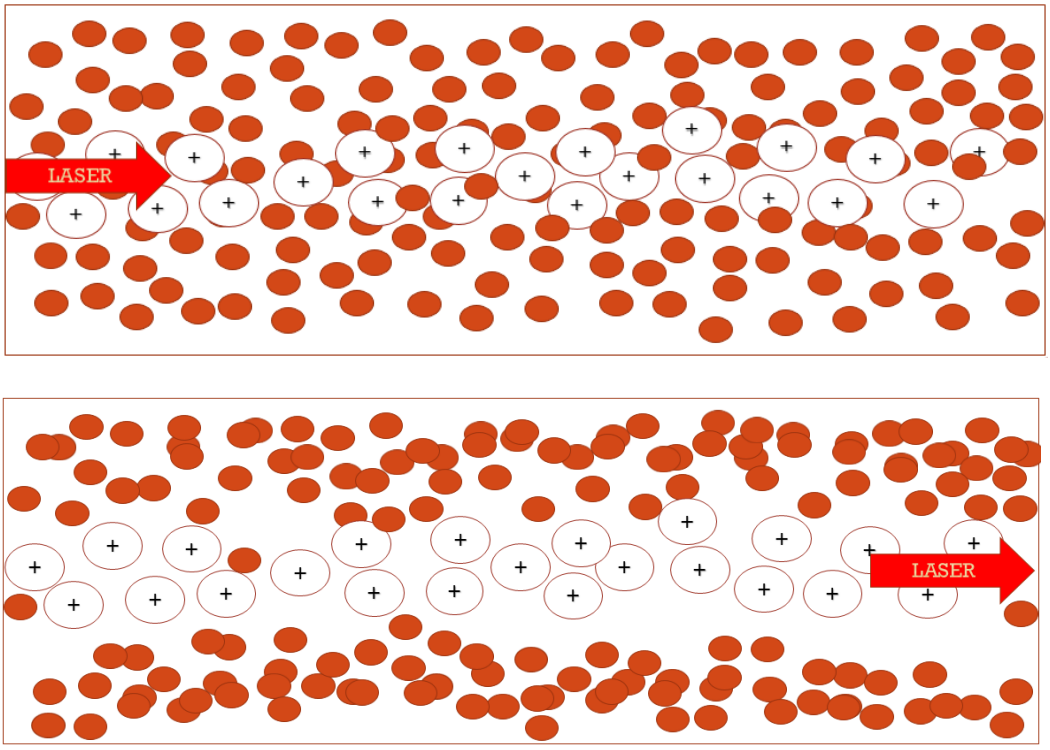

Fig.4.1 (color)

(a) Plasma electrons are at equilibrium before LASER propagation

(b) Plasma electrons are pushed from axial region due to Ponderomotive force after Laser Pulse

In the 3D nonlinear regime, the leading-order transverse motion of the electron fluid is still the quiver motion, $p_\perp = a_\perp$, and $p_\perp \, and \, a_\perp \; are \; normalized \; to \; mc$. And assuming that the laser pulse is propagating in an underdense plasma and has a sufficiently broad spot size, $r_0 \geq \lambda_p \gg \lambda$.

Defining $\delta p = p - a$, the fluid momentum equation can be written as [13] [14] [15]

$$\frac{\partial \delta p}{\partial t} = \nabla(\emptyset - \gamma) \qquad \ldots (4.17)$$

Here $\nabla\emptyset$ is the space-charge force and $\nabla\gamma$ represents the generalized nonlinear ponderomotive force;

4.2 WAKEFIELD GENERATION

As now we have established that, the nonlinear Ponderomotive force is the driving force behind the Plasma Wakefield generation. As an intense Laser beam is passed through the plasma medium, the Ponderomotive force will be high enough to create a perturbation of the electron density along the propagation direction.

Considering n_0 is the equilibrium density of plasma before propagation of laser pulse, If the perturbation generated in the density due to the Ponderomotive force is δn, in linear regime both $n_0 \; and \delta n$ will satisfy equation of continuity, equation of motion and Poisson's equation.

$$Equation \; of \; continuity: \quad \frac{\partial \, \delta n}{\partial t} + \, n_0 \vec{\nabla}.\vec{v} = 0 \qquad \ldots (4.18)$$

$$Equation \; of \; motion: \quad \frac{\partial \vec{v}}{\partial t} = \frac{e}{m}\frac{\partial \vec{A}}{\partial t} - \frac{e^2}{2m^2}\vec{\nabla}A^2 \qquad \ldots (4.19)$$

$$Poisson's \text{ equation}: \quad \vec{\nabla}.\frac{\partial \vec{A}}{\partial t} = \frac{e}{\varepsilon_0}\delta n \qquad \ldots (4.20)$$

Taking $\vec{\nabla}.$ on both sides of equation (4.19), we get

$$\vec{\nabla}.\frac{\partial \vec{v}}{\partial t} = \frac{e}{m}\vec{\nabla}.\left(\frac{\partial \vec{A}}{\partial t}\right) - \frac{e^2}{2m^2}\vec{\nabla}.\left(\vec{\nabla}A^2\right) \qquad \ldots (4.21)$$

Now from equation (4.20) putting the value of $\vec{\nabla}.\frac{\partial \vec{A}}{\partial t}$ in equation (4.21), we obtain,

$$\frac{\partial(\vec{\nabla}.\vec{v})}{\partial t} = \frac{e^2}{m\varepsilon_0}\delta n - \frac{e^2}{2m^2}\vec{\nabla}.\left(\vec{\nabla}A^2\right) \quad \ldots(4.22)$$

From equation (4.18), the value of $\vec{\nabla}.\vec{v}$ is found to be $-\frac{\partial}{\partial t}\left(\frac{\delta n}{n_0}\right)$, Putting this value in equation (4.22), we obtain,

$$-\frac{\partial^2}{\partial t^2}\left(\frac{\delta n}{n_0}\right) = \frac{e^2}{m\varepsilon_0}\delta n - \frac{e^2}{2m^2}\vec{\nabla}.\left(\vec{\nabla}A^2\right)$$

$$-\frac{\partial^2}{\partial t^2}\left(\frac{\delta n}{n_0}\right) = \frac{n_0 e^2}{m\varepsilon_0}\left(\frac{\delta n}{n_0}\right) - \frac{e^2}{2m^2}\vec{\nabla}^2 A^2$$

$$\left[\frac{\partial^2}{\partial t^2} + \frac{n_0 e^2}{m\varepsilon_0}\right]\left(\frac{\delta n}{n_0}\right) = \frac{e^2}{2m^2}\vec{\nabla}^2 A^2$$

$$\left[\frac{\partial^2}{\partial t^2} + {\omega_p}^2\right]\left(\frac{\delta n}{n_0}\right) = \frac{e^2}{2m^2}\vec{\nabla}^2 A^2 \quad \ldots(4.23)$$

where $\omega_p = \sqrt{\frac{n_0 e^2}{m\varepsilon_0}}$, Electron plasma frequency. As the equation (4.23) suggests, the L.H.S is the perturbation caused in plasma density, and R.H.S is the cause of the perturbation i.e. Ponderomotive force.

The solution to equation (4.23) gives the analytical expression for Wakefield and density perturbation: [16] [17] [18]

$$\vec{E}(\vec{r},t) = -\frac{e.\omega_p}{2m}\int_0^t dt'\, Sin\left(\omega_p(t-t')\right).\vec{\nabla}A^2(\vec{r},t') \quad \ldots(4.24)$$

$$\frac{\delta n}{n_0} = -\frac{1}{\omega_p}\int_0^t dt'\, Sin\left(\omega_p(t-t')\right).\vec{\nabla}^2 A^2(\vec{r},t') \quad \ldots(4.25)$$

The equation (4.24) can further be rewritten in terms of Laser electric field (E_0), where $E_0 = \frac{m.\omega_p}{e}$

$$\frac{\vec{E}(\vec{r},t)}{E_0} = -\int_0^t dt'\, Sin\left(\omega_p(t-t')\right).\vec{\nabla}A^2(\vec{r},t') \quad \ldots(4.26)$$

The solution is mainly a wave of frequency ω_p gives rise to an electric field wave called Plasma Wakefield. It also contains a very fast oscillating part at twice the frequency of the laser beam because of the $\vec{\nabla}^2 A^2$term.

The equation (4.24) and (4.26) suggests that Wakefields will be generated most efficiently when the envelope scale length, which characterizes the axial gradient in normalized laser intensity A^2, is of the order of plasma wavelength λ_p. The radial extension of the Wakefield is of the order of the laser spot size r_0.

When $\vec{E} \ll E_0$ (Linear regime,${a_0}^2 \ll 1$), the plasma wave is sinusoidal in nature oscillating with frequency ω_p. But when $\vec{E} \gg E_0$ (Non-linear regime, ${a_0}^2 \gg 1$), the above equations are invalid as the plasma wave becomes more of a Sawtooth signal than sinusoidal. As ${a_0}^2 \gg 1$, the laser beam becomes relativistic in nature, so we have to assume that the laser is non-evolving and only a function of the co-ordinate $\xi = \mathrm{z} - v_p t$,where ξ is the co-moving variable and $v_p \leq c$ is the phase velocity of plasma wave. Using quasistatic approximation, the plasma fluid quantities are also assumed to be function of co-moving variable ξ [19] [20].

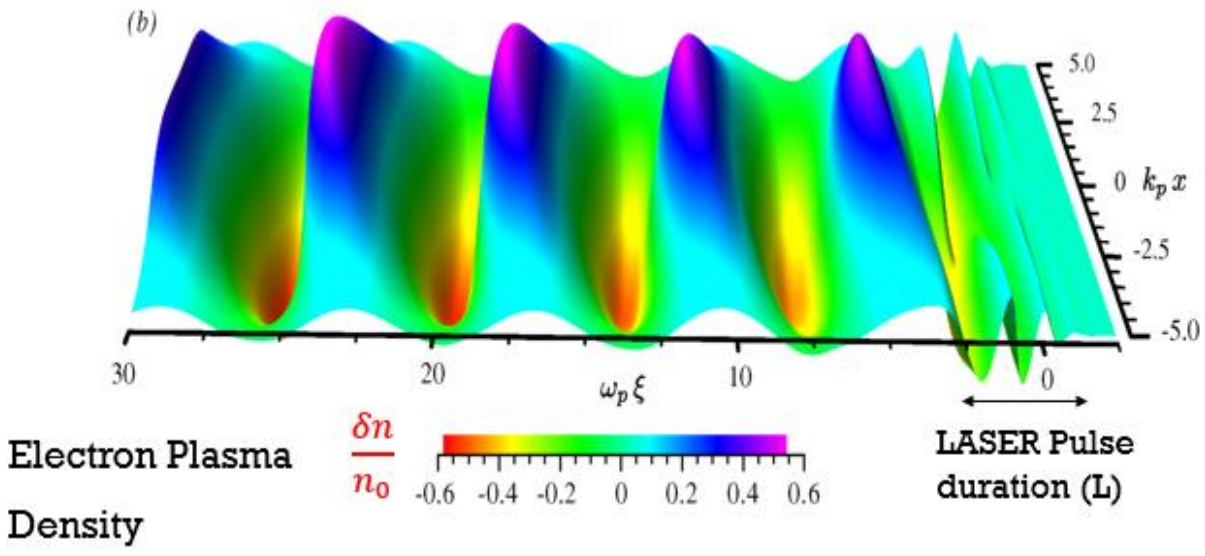

Fig 4.2 (color): Plasma Wakefield Generation

[Advanced Acceleration Technique, By Carl B. Schroeder (LBNL), 26th International Symposium on Lepton Photon Interactions at High energies, June 24-29, 2013]

The Poisson's equation can be written as [19]

$$\frac{\partial^2 \emptyset}{\partial \xi^2} = {k_p}^2 \left(\frac{n}{n_0} - 1\right) \quad \ldots (4.27)$$

Applying quasistatic approximation the above equation can be rewritten as [20] [21]

$${k_p}^{-2} \frac{\partial^2 \emptyset}{\partial \xi^2} = {\gamma_p}^2 \left\{ \beta_p \left[1 - \frac{{\gamma^2}_{\perp}}{{\gamma_p}^2 (1 + \emptyset^2)} \right]^{-\frac{1}{2}} - 1 \right\}, \quad \ldots (4.28)$$

where $\gamma_\perp^2 = 1 + v_\perp^2 \approx 1 + a^2$, ${\gamma_p}^2 = \frac{1}{\sqrt{1-\frac{v^2}{c^2}}}$, $\beta_p = \frac{v}{c}$, $\emptyset = Scalar\ electrostatic\ potential$

In relativistic limit [20] [21] [22], ${\gamma_p}^2 \gg 1, {k_p}^{-2} \frac{\partial^2 \emptyset}{\partial \xi^2} = \frac{(1+a^2)}{2(1+\emptyset^2)} - \frac{1}{2}$ ... (4.29)

The solution to equation (4.29) suggests that the plasma wave steepens and its period lengthens. And the electric field exhibits the characteristics "Sawtooth" profile and the density perturbation becomes more peaked as the Laser intensity increases.

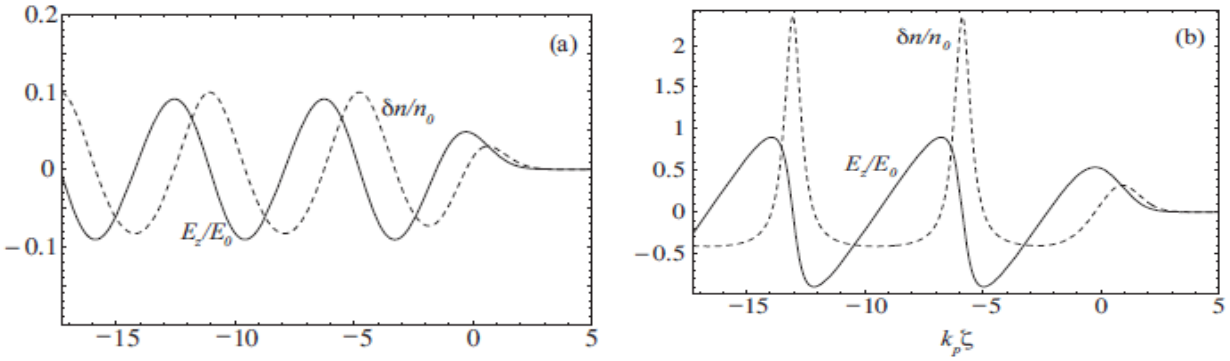

Fig 4.3 Timed average Density perturbation $\left(\frac{\delta n}{n_0}\right)$ (dashed curve) and axial electric field of Plasma Wake$\left(\frac{\vec{E}(\vec{r},t)}{E_0}\right)$ (Solid curve) in [23]

(a) Linear limit; ${a_0}^2 \ll 1$

(b) Non-linear limit; ${a_0}^2 \gg 1$

This is an important parameter in plasma based accelerator and will be useful in accelerating charged particle, which will be discussed in later chapter.

By solving equation (4.29) we get the non-linear plasma wavelength in relativistic limit and is given by

$$\lambda_{NP} = \left(\frac{2}{\pi}\right)(1 + \emptyset_{max})^{\frac{1}{2}}.E_2(\varrho) \qquad \ldots(4.30)$$

Where $E_2(\varrho) = \int_0^{\frac{\pi}{2}} d\theta.(1 - \varrho^2 Sin^2\theta)^{\frac{1}{2}}$ is complete elliptical integral of second kind with argument $\varrho^2 = 1 - \frac{1}{(1+\emptyset_{max})^2}$.

By substituting the value of elliptic integral, the nonlinear plasma wavelength is found to be [20] [21] [22] [24]

$$\lambda_{NP} = \lambda_P.\begin{cases} 1 + \dfrac{3\left(\frac{E_{max}}{E_0}\right)^2}{16}, & E_{max}/E_0 \ll 1 \\ \left(\dfrac{2}{\pi}\right)\left(\dfrac{E_{max}}{E_0} + \dfrac{E_0}{E_{max}}\right), & E_{max}/E_0 \gg 1 \end{cases} \qquad \ldots(4.31)$$

The increase in the plasma wavelength with increasing wave amplitude has an additional effect on nonlinear 3D plasma waves. For a plasma wave that is driven by a Gaussian laser pulse, where the laser intensity peaks on axis. On axis, the plasma wave amplitude is maximum and, in the nonlinear regime, the plasma wavelength on axis is larger than off axis. Thus the plasma wavelength varies as a function of radius $\lambda_{NP}(r)$. This causes the wave fronts of the plasma wave to become curved and take on a "horseshoe" shape. The farther back within the plasma wave train, the more curved plasma wave front is. This curvature of plasma wave fronts lead to transverse "wave breaking".

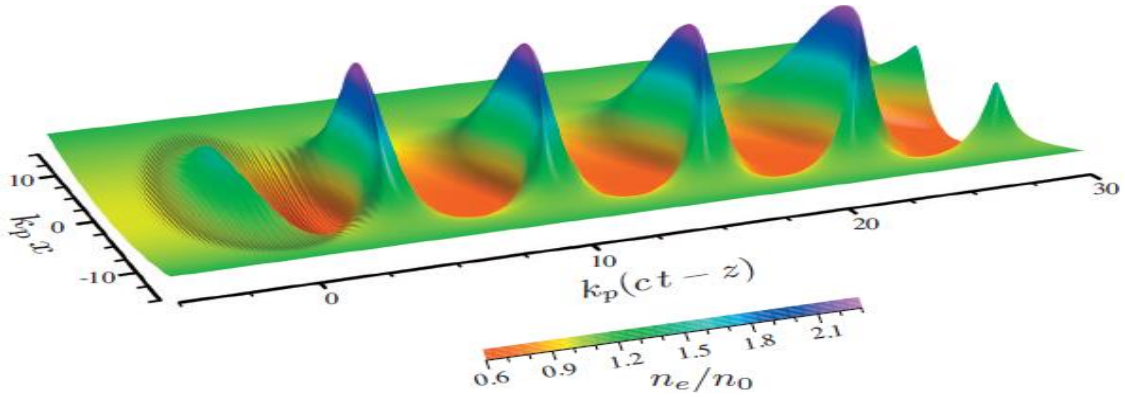

Fig 4.4: Plasma density perturbation excited by a Gaussian Laser pulse traveling a_0 = 1.5

4.3 WAVE BREAKING

The wave breaking in plasma occurs when the maximum amplitude of nonlinear plasma wave exceed the value of E_0.

To understand the Wave breaking phenomena in plasma, an excellent analogy can be made to the rising waves in the ocean. As the waves reach their peak points, they tend to converge on themselves. And same thing happens in Plasma too when excited by a sufficiently strong laser.

Fig 4.5

In the linear regime, the electric field of plasma wave has the form of

$$E_z = E_{max}.Sin\left[\omega_p\left({}^{z}/_{v_p} - t\right)\right],$$

where $v_p = phase\ velocity$ and Z is the propagating direction.

The peak field amplitude $E_{max}$of the plasma wave can be estimated from the Poisson equation. A simple estimate for the maximum field amplitude is given by assuming all plasma electrons are oscillating with a wave number $k_p = \frac{\omega_p}{c}$. This gives

$$\left(\frac{\omega_p}{c}\right).E_{max} = 4\pi e n_0$$

$$E_{max} = \frac{4\pi e n_0 c}{\omega_p} = E_0 \qquad \ldots (4.32)$$

This is the cold non-relativistic wave breaking limit. But in case of nonlinear plasma wave, it is possible for the maximum amplitude to exceed the value of E_0. By using the 1D-nonlinear, relativistic, cold fluid equations the maximum amplitude of periodic plasma wave [25] [26] is

$$E_{WB} = \sqrt{2}\left(\gamma_p - 1\right)^{\frac{1}{2}} E_0, \qquad \ldots (4.33)$$

where $\gamma_p \left(= \frac{1}{\sqrt{1-\frac{v_p^2}{c^2}}}\right)$ is the relativistic Lorentz factor

This is the Cold relativistic wave breaking limit.

But as the wave approaches ultra-relativistic limit ($v_p \approx c$), cold fluid theory will not be valid anymore and we have to use warm fluid model. And the wave breaking limit [27] is found to be

$$E_{WB} \sim \frac{E_0}{\sqrt{\beta_{th}}} \qquad \ldots (4.34)$$

where $c\beta_{th}\left[= \left(\frac{k_B T_0}{m}\right)^{1/2}\right]$ *is the thermal velocity spread of plasma eletcron.*

Equation (4.32), (4.33) and (4.34) are based on 1D theory. Calculation of Wave breaking limit in 3D is not possible in analytical solution and generally calculated through PIC algorithms.

Another advantage of wave breaking is, it assists in trapping electron for acceleration. This will be discussed in further chapters.

4.4 PARTICLE TRAPPING

The dynamics of an electron in the presence of plasma wave and a laser pulse is determined by the Hamiltonian in the co-moving frame [28]

$$H(\tilde{p}, \xi) = (\gamma^2 + \tilde{p}^2)^{1/2} - \beta_p \tilde{p} - \emptyset(\xi), \qquad \ldots (4.35)$$

where $\emptyset(\xi) = plasma\ wave\ space\ charge\ potential,$

$\tilde{p} = electron\ momentum\ normalized\ to\ mc.$

Equation (4.35) gives the normalized particle energy in the co-moving wave frame. The Hamiltonian is time independent, so $H(\tilde{p}, \xi) = constant$ ... (4.36)

The Hamiltonian for separatrix is given by

$$H_s = \frac{\gamma_{\perp}(\xi_m)}{\gamma_{\emptyset}} - \emptyset(\xi_m), \qquad \ldots (4.37)$$

where $\xi_m = phase\ that\ maximises\ the\ H(\tilde{p}, \xi)$,

$\emptyset(\xi_m) = \emptyset_{min}, Minimum\ potential\ which\ will\ be\ at\ peak\ electric\ field.$

The orbit of the electron will be defined by the Hamiltonian

$$H_t = (1 + \tilde{p}_t^{\,2})^{1/2} - \beta_p \tilde{p}_t \qquad \ldots (4.38)$$

By solving for, $H_s = H_t$, the minimum momentum required for electron trapping is found to be

$$\tilde{p}_t = \gamma_p \beta_p \left(\gamma_{\perp} - \gamma_p \emptyset_{min}\right) - \gamma_p \left[\left(\gamma_{\perp} - \gamma_p \emptyset_{min}\right)^2 - 1\right]^{\frac{1}{2}} \qquad \ldots (4.39)$$

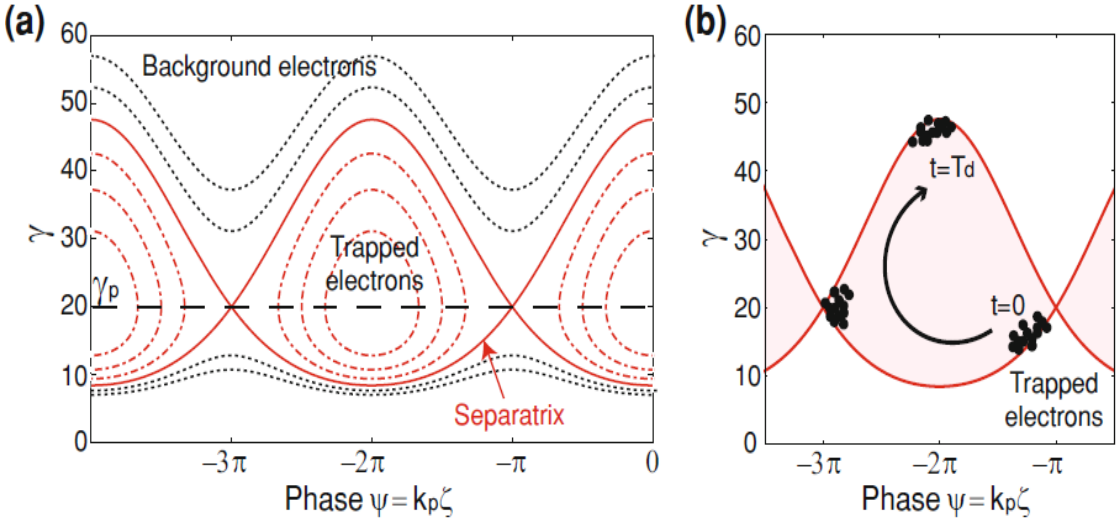

Fig 4.6 (color): single electron orbits (dotted curves), separatrix (solid curve), and the dashed curve is the cold fluid orbit (dashed curve)

[Investigation of staged Laser Plasma Acceleration, S. Shiraishi, 2015, XVII, Pg.121]

(a) Shows an example of single electron orbits in $(\tilde{p}, \xi)$ phase space. Electron with too little or too much energy are represented with black dotted curve while trajectory of trapped electrons are shown with red dotted curve. The solid curve is the separatrix. The dashed curve is the cold fluid orbit, i.e., an electron initially at rest.

(b) Shows acceleration of trapped electron in momentum phase space. Initially low energy electrons at t=0 outruns the plasma wave at $t=T_d$.

This is the Trapping condition for electron in a Wakefield.

For $H_t > H_s$; the electron will be in untrapped orbit.

For $H_t \leq H_s$; the electron will be in trapped orbit.

The threshold momentum required for trapping decreases for larger plasma wave amplitude a for lower plasma wave velocity. The curvature of plasma wave fronts can enhance trapping into the focusing and accelerating region as discussed in wave breaking chapter before [29].

For cold plasma, all electron momentum $\tilde{p}_t = 0$ and $H_t = 1 = H_{cold}$.

And to obtain trapping condition for cold electron, $H_{cold} = H_s$. And the trapping condition obtained is $E_m = \sqrt{2}(\gamma_p - 1)^{\frac{1}{2}} E_0$. This is same as our wave breaking condition in cold plasma fluid theory as described in equation (4.33). So it can be said that wave breaking phenomena assists in electron trapping.

The same concept can be understood from the electron velocity point of view. If its initial velocity is too low, the electron won't gain enough velocity to catch up the phase of the Wakefield and will slip backward the wave to a decelerating phase region. But if the electron has a high enough initial velocity, it will outrun the Wakefield wave and slip forward it to a decelerating phase region, which will lead it to be trapped in the Wakefield wave. One can make an analogy with a surfer who manages to catch a wave and use it to accelerate.

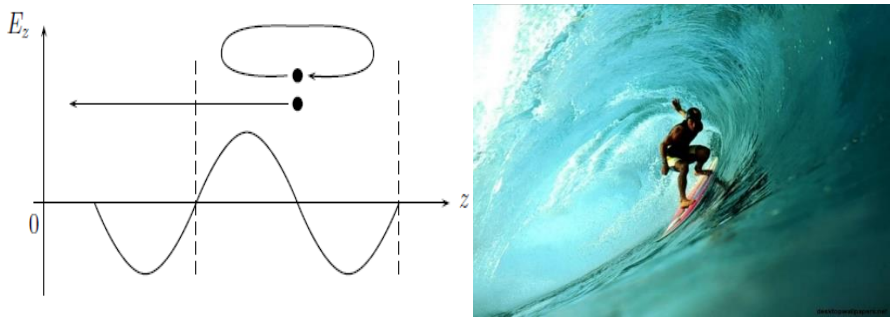

(a) (b)

Fig 4.7 (color) (a) Electron trapping. The upper dot represents an electron trapped within the dashed lines, the lower dot represents an untrapped electron which slips backward the wave. (b) Surfer (electron) trapped inside a rising ocean wave (Wakefield) as the wave converges (wave breaking) on itself.

CHAPTER V

5. ACCELERATION IN THE BUBBLE REGIME

5.1 THE BUBBLE REGIME

The idea behind the plasma accelerators is to use the longitudinal component of the Wakefield to accelerate the electrons. As solution of equation (4.24) shows that the amplitude of the longitudinal Wakefield is maximum when the length of the laser pulse (L) is approximately equal to the plasma wavelength (λ_p). The order of magnitude of the maximal Wakefield amplitude is given by equation (4.33) in relativistic limit. Let's consider an example just to show the accelerating gradient a Plasma accelerator can achieve, for a plasma density of $n_0 = 10^{24} m^{-3}$, the accelerating gradient is:

$$\omega_p = \left(\frac{n_0 e^2}{m\varepsilon_0}\right)^{0.5} = 5.6334 \times 10^{13} \frac{rad}{s}$$

From Poisson's equation the maximum gradient can be found by $E_{max} = \frac{e n_0 c}{\varepsilon_0 \omega_p} \approx 100\ GV/m$ which is almost 10^4 times the typical electric field in the conventional accelerators. To generate maximum Wakefield the laser pulse length (L) must be of the order of plasma wavelength (λ_p).

$$L \sim \lambda_p \approx \frac{3.3 \times 10^{10}}{\sqrt{n_o (cm^{-3})}} = 33 \mu m$$

So Laser pulse duration $= {}^{\text{Laser pulse length}}/_{c} \approx 100 fs$

The basic physics behind the laser driven plasma acceleration is, the short laser pulse consists in a propagating spot which will expel electrons on its way because of the ponderomotive force. If the laser intensity is very high, so that it expels all the electrons from the axis and forms an electron deprived regime, usually called the "*Bubble, Blow-out or cavitation regime".* And due to the wave breaking, the background electrons are trapped inside the bubble. The strong resulting electric field of the bubble region will accelerate the electrons, resulting in the creation of an electron beam which follows the laser spot, without being disturbed by the laser electromagnetic field. Some features of the bubble region are,

(i) the cavity is free from cold plasma electrons is formed behind the laser pulse instead of a periodic plasma wave

(ii) a dense bunch of relativistic electrons with a monoenrgetic spectrum is self-generated

(iii) the laser pulse propagates many Rayleigh lengths in the homogeneous plasma without a significant spreading

Although LWFA was the first type of plasma accelerator to be developed, the formation and physics of the bubble regime was first studied by A. pukhov and J. meyer-ter-vehn in 2002 [30], because all the LWFA experiments before are done by non-relativistic laser driver. As now high power laser have been developed, which can be operated in relativistic regime, the formation of bubble region is noticed.

The electrons are trapped inside the bubble due to the wave breaking of plasma Wakefield, described by equation (4.33). This phenomenon is called self-injection. The bubble region cannot be described by the linear plasma theory, this is why numerical simulations are required to study the physics of bubble region.

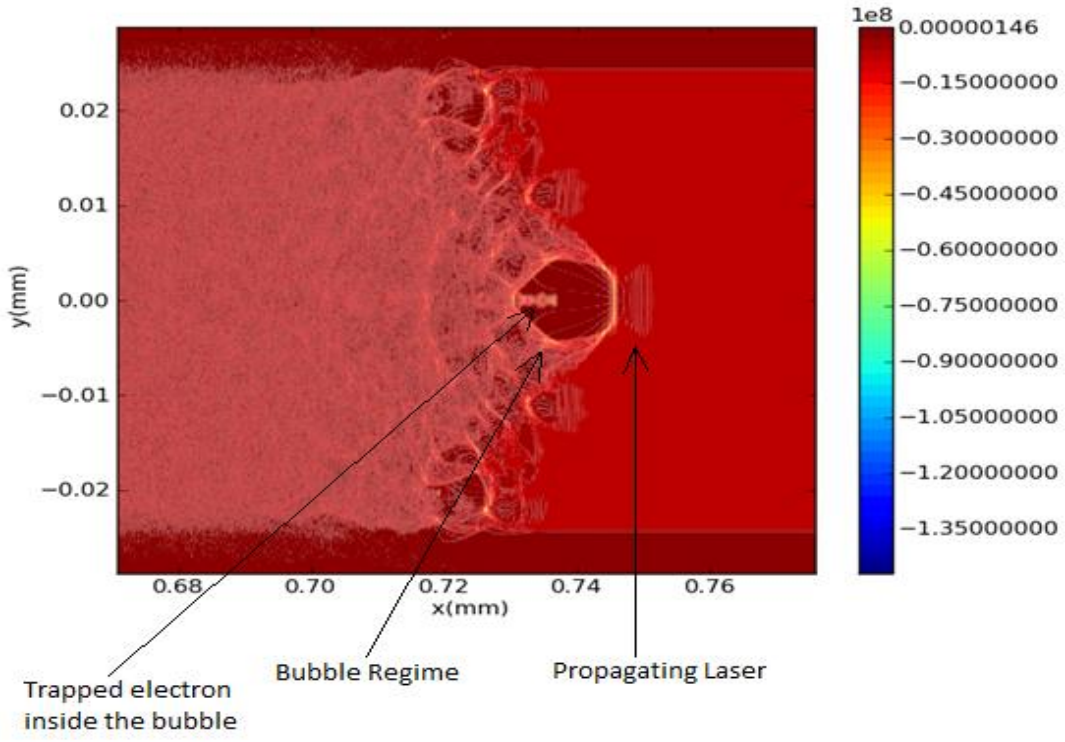

Fig.5.1 (color): Shows the trapped electron inside a plasma bubble of nominal plasma density of 4×10^{25} m^{-3} driven by a laser of $a_0 = 4.0$, laser Spot size of 8.5μm and the wavelength of the laser is 0.8μm

The bubble region as shown in the figure 5.1 can be divided into 3 parts.

(a) The cavity region deprived of electrons

(b) The skin of the bubble composed of electrons which forms the boundary of the bubble

(c) And the trapped electrons inside the bubble those are accelerated due to the axial electric field of the bubble.

The density of the boundary of the bubble is the highest at the head and base of the bubble, and minimum at the middle. At the head and base the bubble have maximum number of relativistic electrons those have the same velocity as the bubble. And the base of the bubble acts as the source of electrons which are trapped in the bubble to be accelerated.

The bubble regime is formed when the laser pulse length has the value to form maximum Wakefield and at which point the wave breaking will occur. For a Gaussian pulse profile the maximum Wakefield will be formed when the Full width half maximum of laser pulse (L_{FWHM}) is 37% of the plasma wavelength (as given in Table 3.1).

For a Gaussian pulse profile, $a^2 = {a_0}^2 . \exp\left(\frac{-2r^2}{{r_0}^2}\right)$, on the axis ($R_B = 0$), density is

$$\frac{n(0)}{n_0} = 1 - \frac{4}{{k_p}^2 {r_0}^2} \frac{{a_0}^2}{(1 + {a_0}^2)^{\frac{1}{2}}} \quad \ldots (5.1)$$

For complete bubble to be formed, the electron density inside the bubble must be zero, i.e. $n(0) = 0$. By putting this condition, we find that

$$\frac{{a_0}^2}{(1 + {a_0}^2)^{\frac{1}{2}}} \geq \frac{{k_p}^2 {r_0}^2}{4} \quad \ldots (5.2)$$

For relativistic limit, ${a_0}^2 \gg 1$, so eqution 5.2 transforms to $a_0 \geq \frac{{k_p}^2 {r_0}^2}{4}$. From this the condition for laser to form a bubble during propagation in plasma [30] is

$$r_o \leq \frac{2}{k_p} \sqrt{a_0} \quad \ldots (5.3)$$

For optimal wake generation the laser must satisfy following condition

$$r_o k_p \approx \sqrt{a_0} \quad \ldots (5.4)$$

$$\tau \leq \frac{r_0}{c} \quad \ldots (5.5)$$

$$\text{And Power } P(GW) > 30 \left[\frac{\tau(fs)}{\lambda(\mu m)}\right]^2 \quad \ldots (5.6)$$

Equation 5.3 is established according to 3D phenomenological non-linear theory [30] ($a_0{}^2 \gg 1$), according to linear ($a_0{}^2 \ll 1$) and 1D non-linear theory ($a_0{}^2 \gg 1$) the bubble radius (R_B) remains constant as well as the spot size of the laser.

$$r_o k_p = 2\pi \qquad \ldots (5.7)$$

5.2 SHAPE OF THE BUBBLE

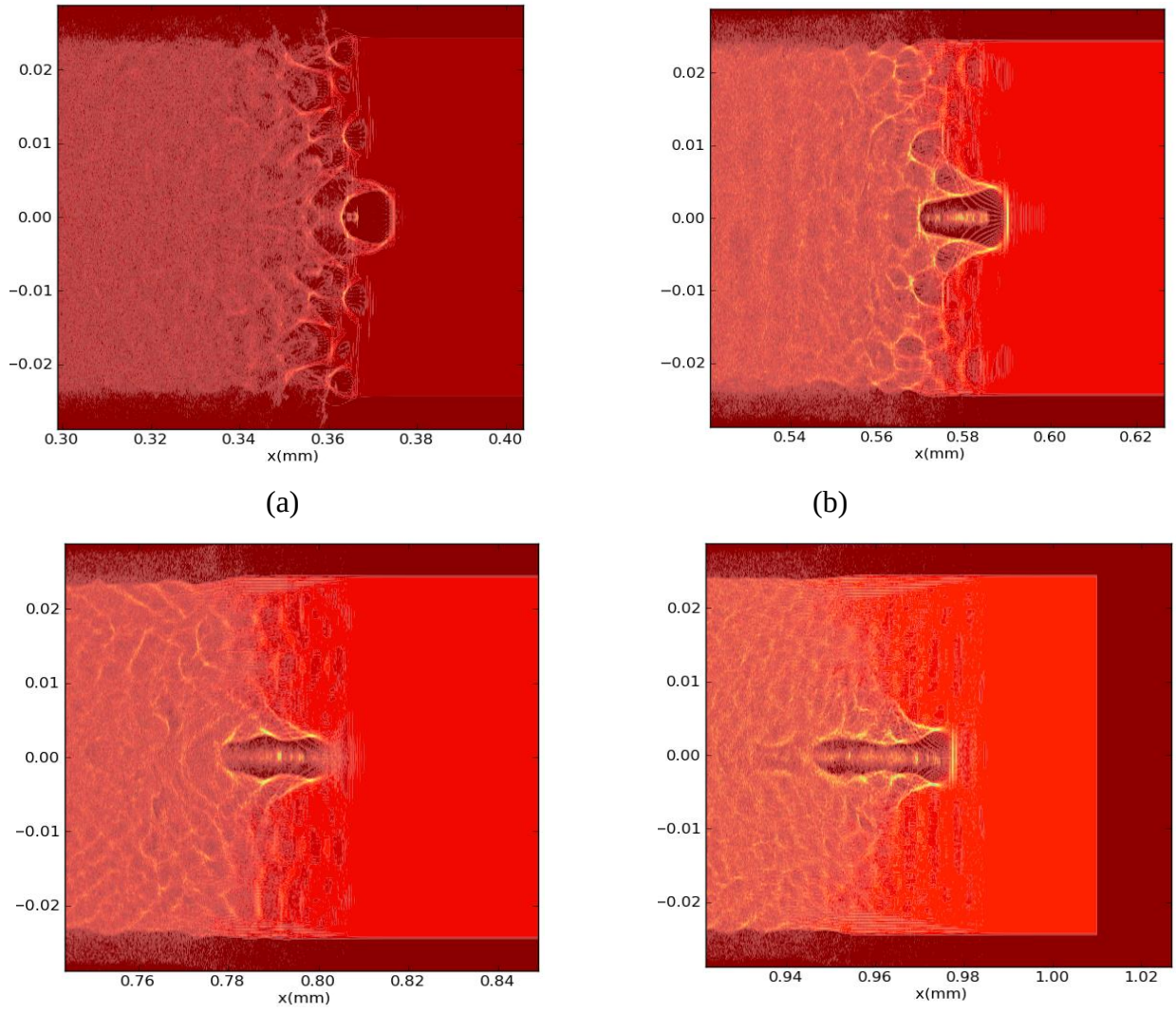

Fig 5.2 (color): The shape of the bubble at (a) 370μm (b) 570μm (c) 780μm (d) 950μm

The laser having a_0=4.0, spot size of 8.5μm and wavelength of 0.8μm is moving in X-direction through a uniform plasma density of 4×10^{25} m^{-3}

From the equation 5.3, the radius of the bubble, assuming the bubble has a spherical symmetry, can be defined as

$$R_B \approx \frac{2}{k_p}\sqrt{a_o} \quad \ldots (5.8)$$

To achieve a complete spherical symmetry, for lasers having $a_0 \geq 4$, the power and plasma density conditions are as given below:

$$P(GW) \approx 21.5\left(\frac{a_0 R_B}{\lambda}\right)^2 \quad \ldots (5.9)$$

$$2 \times 10^{25} \geq n \geq 2 \times 10^{24} m^{-3} \quad \ldots (5.10)$$

The electrons inside the bubble are being subjected to huge electric field of bubble and accelerated in the longitudinal direction of laser propagation. The electric field inside the bubble is maximum at the start of the bubble and weakens as the bubble lengthens. The middle of the Bubble has the lowest field. So after the electron passes the midpoint of the bubble, it starts to decelerate and become out of phase with the accelerating field of the bubble. This phenomenon is called electron dephasing and will be described in next chapter in detail.

5.3 CHARACTERISTICS OF BUBBLE REGIME

The accelerating field inside the bubble regime is divided into transverse and longitudinal field. The transverse field (radial) is almost constant and is function of the radius of the bubble. The longitudinal field (Axial) which accelerates the electron varies linearly with the distance behind the laser pulse. Along with the accelerating field, a focusing field, which characterizes the output beam emittance, is a function of radius and varies linearly.

Assuming the bubble regime is spherical in nature, with a radius (R_B) centered and $r = 0\ and\ \xi = 0$, moving at relativistic velocity [30]

The Axial electric field: $$E_z \approx \left(\frac{k_p \xi}{2}\right) E_0 \quad \ldots (5.11)$$

The Radial Electric Field $$E_r \approx \left(\frac{k_p r}{4}\right) E_0 \quad \ldots (5.12)$$

The Azimuthal Magnetic Field $$B_\theta \approx -\left(\frac{k_p r}{4}\right) E_0 \quad \ldots (5.13)$$

The axial electric field is maximum when $\xi = R_B$.

The transverse Wakefield is electromagnetic such that the radial focusing force on a relativistic electron moving along the axis is

$$F_r = E_r - B_\theta = \left(\frac{k_p R_B}{2}\right) E_0 \quad \ldots (5.14)$$

The focusing force of the bubble region is very large and linear in nature, so the emittance of the accelerated electron bunch is preserved. The radial electric field at the edge of an electron beam with the radius of bubble $R_{B,}$

$$E_r \left(\frac{MV}{m}\right) = 9.06 \times 10^{-15}\, n(cm^{-3}) R_B(\mu m) \quad \ldots (5.15)$$

The radial force causes the accelerated electron at relativistic limit to perform betatron oscillations about the axis with betatron wavelength $\lambda_\beta = \sqrt{2\gamma}\lambda_p$ (Esarey et al. 2002). As the beam radiates, the energy spread of the output of the beam will increase and mean energy will decrease [32]. And this radiation can fall in the X-ray region, causing the plasma accelerator to release X-ray.

5.4 PARTICLE TRAPPING IN THE BUBBLE

Assuming the bubble has a spherical shape, the trapping condition for electron by the bubble traveling at a relativistic velocity is derived by Kostyukov et. al in Jan 2009 [33]. The electron dynamics in the bubble is defined by the Hamiltonian

$$H = \sqrt{1 + (P + a)^2 + {a_0}^2} + \emptyset\,, \quad \ldots (5.16)$$

where $P = Canonical\ momentum\ of\ the\ electron$

$a = Vector\ potential$

$a_0 = Normalized\ Vector\ potential$

$\emptyset = Scalar\ potential\ inside\ the\ bubble$

The transverse motion of electron is neglected and the acceleration trajectory is in XY-plane. As shown in the figure 5.3, the electron is at the start of the bubble at y=R_B and $\xi = 0$, which is the injection point at the base of the bubble. As the electron reaches trapping point where $\xi =$ R, and y=0, the forward velocity of the electron must be greater than Wakefield phase velocity.

As suggested by I. Koshyukova et. al, 2009 [33] the condition for trapping is

$$\gamma_e \leq \frac{R_B}{\sqrt{2}} \qquad \ldots (5.17)$$

where γ_e *is the lorentz factor of the electron trapped.*

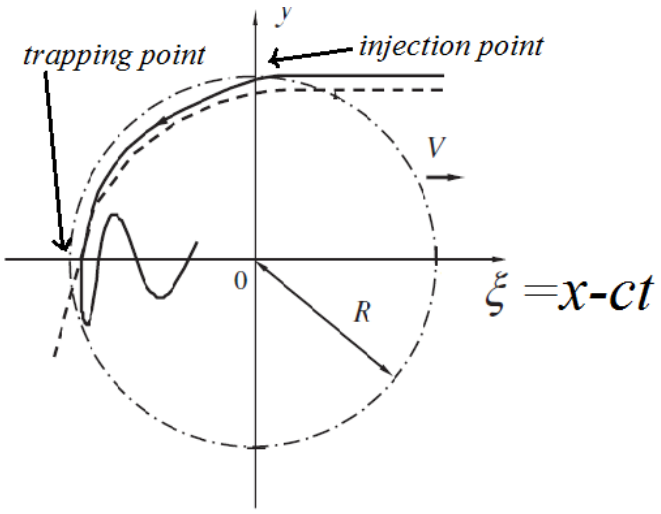

Fig 5.3 trajectory of trapped (solid line) and untrapped (dashed line) electron

After the electron is trapped inside the bubble the electron remains trapped due to the transverse field of the bubble and accelerated towards the propagation axis.

5.5 ACCELERATION INSIDE THE BUBBLE

To find the number of electrons trapped inside a bubble and the energy gained by them, scaling laws have to be derived [34] [35].

The relativistic similarity parameter

$$S = \frac{{k_p}^2}{a_0\, k^2} = \frac{n_e}{a_0\, n_{critical}}\,, \qquad \ldots (5.18)$$

where $n_e = Electron\ plasma\ density\ (as\ described\ in\ Chapter\ II)$

$n_{critical} = Critical\ electron\ plasma\ density\ (as\ described\ by\ equation\ 2.24)$

$a_0 = Normalized\ vector\ potential = \frac{eA}{mc^2}$

The relativistic similarity parameter is a dimensionless parameter. As it can be seen from equation 5.18 for a relativistically underdense plasma $S \ll 1$, and for overdensed plasma $S \gg 1$.

The bubble is formed in a relativistically underdense plasma, and the number of monoenrgetic electrons trapped in the bubble are given by [35]

$$N \approx \frac{1.8}{k_0 r_e}\sqrt{\frac{P}{P_{relativistic}}}\ , \qquad \ldots (5.19)$$

where $r_e = classical\ electron\ radius = \frac{1}{4\pi\varepsilon_0}\frac{e^2}{mc^2} = 2.817940326727 \times 10^{-15}\ m$

$P = Laser\ pulse\ power$

$P_{relativistic} = Relativistic\ power\ unit = \frac{m^2c^5}{e^2} = 7.877765742 \times 10^{19}$

$k_0 = laser\ propagation\ vector = \frac{2\pi}{\lambda}$

And the energy gained by the trapped electron is

$$E \approx 0.65mc^2\sqrt{\frac{P}{P_{relativistic}}}\frac{c\tau}{\lambda} \qquad \ldots (5.20)$$

And the electrons need to be accelerated over a length L_{acc} to gain this much energy.

$$L_{acc} = 0.7\frac{c\tau}{\lambda}Z_R\ , \qquad \ldots (5.21)$$

Where $Z_R\ is\ the\ Rayleigh\ length = \frac{k{r_0}^2}{2} = \frac{\pi{r_0}^2}{\lambda}$

CHAPTER VI

6. ACCELERATION LIMITS IN LWFA

The energy gain by an electron in a laser driven plasma accelerator is determined by laser plasma interaction length, which is roughly estimated by the product of Wakefield amplitude and effective acceleration length. There are several mechanisms those can limit the energy gain by a particle in LWFA: Laser Diffraction, Electron Dephasing, Pump Depletion, and Laser-Plasma Instabilities.

6.1 LASER DIFFRACTION

The most significant limitation on acceleration length is due to laser diffraction [36]. In vacuum, laser pulse undergoes Rayleigh diffraction such that laser spot size evolves according to

$$r_s = r_0\left(1 + \frac{z^2}{{Z_R}^2}\right)^{\frac{1}{2}}, \qquad \ldots (6.1)$$

where $r_0 = Min\ spot\ size\ at\ focal\ point\ z = 0$

$Z_R = Rayleigh\ length = \frac{k{r_0}^2}{2}$

Without any optical guiding the laser plasma interaction distance will be limited to few Rayleigh lengths [37]. There are various methods of guiding a pulse in plasma,

(a) Refractive guiding

(b) Relativistic optical guiding

(c) Plasma wave guiding

(d) Guiding through performed plasma density channel

Extension of laser plasma interaction length has been achieved by combination of performed plasma channel guiding, relativistic self-focusing and ponderomotive self-channeling enabling production of extremely high quality electron bunch.

6.2 LASER PUMP DEPLETION

The phenomenon of a laser pulse losing its energy while propagating through plasma driving a Wakefield is called pump depletion. As the Laser driver excites the plasma wave, it loses

energy, or the pump depletes. The pump depletion length can be estimated by using principle of energy conservation theory, i.e., by equating laser pulse energy to energy left behind in the Wakefield. [38] [39]

$$L_{pd} \approx \frac{{\lambda_p}^3}{\lambda^2} \times \begin{cases} \frac{2}{{a_0}^2} & ,for\ {a_0}^2 \ll 1 \\ \left(\frac{\sqrt{2}}{\pi}\right) a_0 & ,for\ {a_0}^2 \gg 1 \end{cases} \quad \ldots (6.2)$$

where a_0 *is the lase strength parameter*

$\lambda_p = wavelength\ of\ plasma\ wakefield$

$\lambda = wavelength\ of\ laser$

Once the pump depletes, staging with fresh pump pulse is required.

6.3 ELECTRON DEPHASING

When the electron is accelerated to high energy, the electron can go faster than the plasma wave and leave the acceleration region; this phenomenon is called dephasing. The dephasing length, denoted by $L_{deph,}$ is defined as the length the electron must travel before its phase slips by one half of a period with respect to the plasma wave. As the accelerated electron outruns the plasma wave, it goes out of phase with the accelerating field and starts to decelerate. The dephasing length is determined by the plasma density, as the electron density decreases the dephasing length increases, and vice-versa. The dephasing length for a square laser pulse profile with linear polarization in 1D limit is [38] [40]

$$L_{deph} = \frac{{\lambda_p}^3}{2\lambda^2} \times \begin{cases} 1 & ,for\ {a_0}^2 \ll 1 \\ \left(\frac{\sqrt{2}}{\pi}\right) \frac{a_0}{N_P} & ,for\ {a_0}^2 \gg 1 \end{cases} \quad \ldots (6.3)$$

N_P *is the number of plasma pulse behind the driver laser pulse.*

In ${a_0}^2 \gg 1$ limit, the factor $\frac{1}{N_P}$ is dominant in determining the plasma wave phase velocity as the plasma wave period increases with steepening of laser pulse.

The electron gain maximum energy when the dephasing length matches the acceleration length, i.e., $L_{deph} = L_{acc}$.

There are various methods to optimize the dephasing length. As $L_{deph} \sim n_p^{-\frac{3}{2}}$, by decreasing the electron density, the dephasing length is increased.

Another method is to use an upward plasma density ramp. With upward density ramp structure, we produce a constantly decreasing plasma wavelength profile, so as the laser propagates through this structure, the accelerating field is always ahead of the plasma wavelength, thus eliminating any chance of dephasing. Another advantage of using an upward density ramp is the maximum energy gained by the electron also increases. In this work, I have used a 2D PIC method to optimize the energy gain through an upward density ramp structure. The simulations and results are discussed in detail in Chapter VIII.

But the effect of dephasing is more prominent in linear regime where $a_0{}^2 \ll 1$, whereas in non-linear regime, where $a_0{}^2 \gg 1$, the effect of pump depletion is dominant. In the linear regime, however, by appropriately tapering the axial plasma density profile, dephasing limitations can be overcome, resulting in a larger single-stage energy gain [41] [42]. By slowly increasing the plasma density as a function of propagation distance, the phase velocity of the Wakefield can be increased. The non-linear regime ($a_0{}^2 \gg 1$) is advantageous as $L_{deph} \sim L_{pd}$, which implies efficient use of pump laser pulse energy in a single stage.

The ideal energy gain in a standard LWFA can be estimated by $\Delta W = eE_z L_{acc}$[41][42], where L_{acc} is the acceleration length and $E_z = E_0 \left(\frac{a_0{}^2}{2}\right)\left(1 + \frac{a_0{}^2}{2}\right)^{-\frac{1}{2}}$ is the maximum electric field amplitude driven by an optimized flat-top, linearly polarized laser pulse in the 1D limit[38][28].

For various acceleration limit, the acceleration length (L_{acc}) and energy gain (ΔW) in practical units are provided in table 6.1

Now let's compare linear theory, 1D non-linear theory and 3D phenomenological nonlinear theory and see the bubble and acceleration phenomenon according to all three of them. As it is described in section 5.1 that according to the linear and 1D non-linear theory the bubble radius remains same, whereas 3D phenomenological theory states that it is scaled according to the value of $\sqrt{a_0}$. And the electron dephasing factor is dominant during acceleration limit only in linear theory whereas the pump depletion governs the acceleration limit in 1D non-linear regime. But in 3D non-linear theory both factors scale the same way. This happens for a reason; in 1D all

the energy of laser is used for wake generation, but in 3D this is not the case. This can be seen in the simulations too.

TABLE 6.1 [42] [43]

ACCELERATION LIMIT	**ACCELERATION LENGTH (L_{acc})**	**ENERGY GAIN (ΔW) in MeV**	
		$a_0^2 \ll 1$	$a_0^2 \gg 1$
LASER DIFFRACTION	$\approx \pi Z_R < L_{deph}, L_{pd}$	$\approx 740 \left(\frac{\lambda}{\lambda_p}\right)\left(1+\frac{{a_0}^2}{2}\right)^{-\frac{1}{2}} P(TW)$	
ELECTRON DEPHASING	$= L_{deph}$	$\approx \frac{630\, I(W/cm^2)}{n(cm^{-3})}$	$\approx \frac{630\, I(W/cm^2)}{n(cm^{-3})}\left(\frac{2}{\pi}\right) N_P$
LASER PUMP DEPLETION	$\approx {L_{pd}}/{2}$	$\approx \frac{3.4\times 10^{21}}{[\lambda(\mu m)]^2\, n(cm^{-3})}$	$\approx \frac{400\, I(W/cm^2)}{n(cm^{-3})}$

6.4 LASER PLASMA INSTABILITIES

Laser-plasma instabilities can limit laser propagation distance and degrade the performance of an LPA. Below are some instabilities associated with short laser pulse

(a) Stimulated Raman scattering (SRS)

(b) Self-modulation

(c) Laser hose instabilities

Stimulated Raman scattering involves interaction of a light wave with electron plasma wave. In this instability, the pump laser pulse decays into an electron plasma wave and two scattered light wave namely a Stokes wave and an anti-Stokes wave. If the pump laser pulse have frequency and wave number as $\omega_0 \, and \, k_0$, respectively, the electron plasma wave have $\omega_e \, and \, k_e$, then the Stokes and anti-tokes wave have frequency and wave number as $(\omega_0 - \omega_e)$, $(k_0 - k_e) and \, (\omega_0 + \omega_e), (k_0 + k_e)$, respectively, electron plasma frequency $\omega_e \approx \omega_p + i\Gamma$, where growth rate Γ can be obtained from linear instability analysis. Self-modulation instability appears due to mutual amplification of the beam radius rippling and the plasma wave [44]. Hose instability occurs when plasma is excited by a long laser pulse, as our work is based mostly on LWFA, which is excited by short relativistic laser pulse, so it is less susceptible to Hose instability.

CHAPTER VII

7. PARTICLE-IN-CELL (PIC) SIMULATION

7.1 INTRODUCTION TO PIC

Before divulging our discussion into PIC method, let's first understand, why PIC is needed? In plasma physics, most of the experiments include large density plasma consisting of at least 10^{23} particles per meter cube. To simulate plasma, we need to track the dynamics of each individual particle. Fluid theory is inadequate to study the behavior of high density plasma. Furthermore our computational cost will increase if we try to simulate each particle individually. PIC method is specially developed to simulate large number of particles.

The force on any particle inside the plasma can be defined through the equation of motion. In plasma the entire particle dynamics and fields can be computed with the help of Maxwell's equation; e.g., 2.7, 2.8, 2.9, 2.10.

Plasma can be visualized by defining the types of interacting system it falls under. There are two types of interacting system

(i) Strongly coupled system

(ii) Weakly coupled system

In strongly coupled system, there are very few number of particles, or we can say; $N_D(= n{\lambda_D}^3)$ is small, where N_D $is\ the\ number\ of\ particles$. So the field is mostly dependent on the average number of collision occurring. The evolution can be determined by the close encounters and relative configuration of any two pairs of particles. The electric field plot is affected by very few number of particles.

In weakly coupled system, the numbers of particles are large; $N_D = n{\lambda_D}^3$ is large. So the collision between particles is negligible. The electric field is not affected by collision rather due to the local concentration of charge. The plot of the electric field will be without much fluctuation compared to the strongly coupled system. In this case the trajectory is affected by large number of particles.

The electrostatic potential energy between two particles with a separation distance 'a' and equal charge 'q' is given by

$$E_{pot} = \frac{q^2}{4\pi\varepsilon_0 a} \quad \ldots (7.1)$$

The kinetic energy of particles is given by

$$E_k = k_B T \quad \ldots (7.2)$$

A measure of plasma coupling is given by the so-called plasma coupling parameter, Λ, defined as

$$\Lambda = \frac{E_k}{E_{pot}} = \frac{4\pi\varepsilon_0 a k_B T}{q^2} \quad \ldots (7.3)$$

$$\Lambda = 4\pi N_D^{\frac{2}{3}} \quad \ldots (7.4)$$

The plasma parameter gives a new physical meaning to the number of particles per Debye cube. When many particles are present in the Debye cube the thermal energy far exceed the potential energy, making the trajectory of each particle little influenced by the interactions with the other particles: this is the case for the weakly coupled systems. Conversely, when the coupling parameter is small, the potential energy dominates and the trajectories are strongly affected by the near neighbour interactions: this is the condition typical of strongly coupled systems.

As the number of particles are less in strongly coupled system, individual particle simulation is somehow feasible, but in case of weakly coupled system, we have to use collective clouds of particles, which represents a group of particles exhibiting similar behavior. They are termed as "*computational particle, super particle or finite size particle*". The advantage of using super particles is that they interact more weakly than point particles. Point particles interact via Coulombian force, which grows as they approach each other and attains singularity as two point particles overlap each other as shown in Fig.7.2

But in case of super particles, they behave as point particle as long as there is no overlapping. Once two super particles overlap, the overlapped area is not responsible for any force. So at fully overlapping condition, the total force between two super particles is zero.

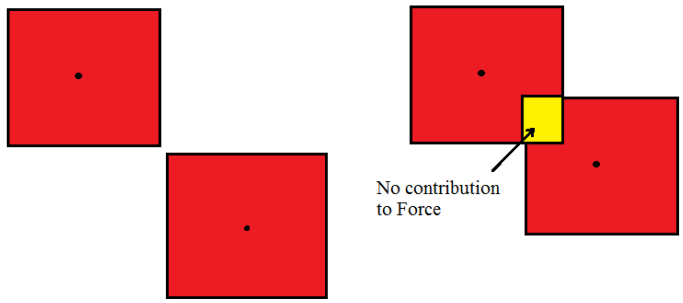

Fig.7.1

The use of super particles allows reducing the interaction among particles. The beneficial consequence is that the correct plasma parameter can be achieved by using fewer particles than in the physical system. The conclusion is that the correct coupling parameter is achieved by fewer particles interacting more weakly. And thus we can define the whole system by defining only a group of particles.

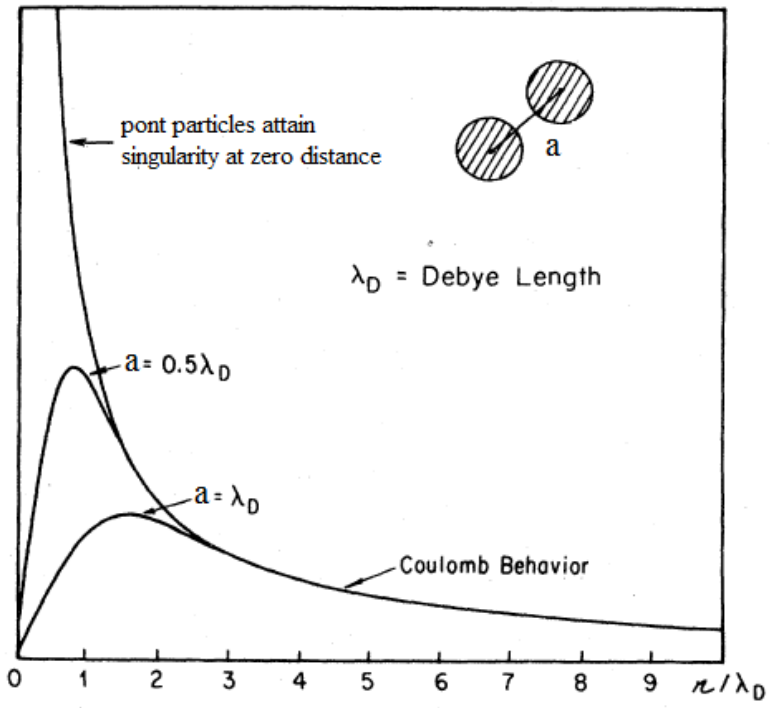

Fig.7.2

(Particle simulations of plasma, John M Dawson [45])

In PIC method, the plasma system is represented by a group of super particles and they are divided into each group such that no super particles are overlapping each other. So the whole

system is free of any collisional force and also able to exhibit behaviour of all the particles in the system.

7.2 MATHEMATICAL DERIVATION

Here, the mathematical derivation for PIC method is done for a 1D electrostatic model. And most of the contents are derived from *R. W. Hockney and J. W. Eastwood. Computer Simulation Using Particles. McGraw-Hill, New York, 1981 and Particle simulations of plasma, John M Dawson* [45]. The phase space distribution function for electrons in plasma can be defined as $f(x, v, t)$. The phase space distribution gives the number density per unit of phase space. The phase space distribution function is governed by the Vlasov equation:

$$\frac{\partial f}{\partial t} + \vec{v}.\nabla f + \frac{\vec{F}}{m}.\nabla_v f = 0.$$

where $\vec{F} = q\vec{E}$.

In 1D limit the Vlasov equation can be written as

$$\frac{\partial f}{\partial t} + v\frac{\partial f}{\partial x} + \frac{qE}{m}\frac{\partial f}{\partial v} = 0\,. \qquad \ldots (7.5)$$

The electric field in electrostatic limit is described by the Poisson's equation

$$\nabla.D = \rho\,.$$

$$\text{1D limit:}\quad \varepsilon_0 \frac{\partial^2 \varphi}{\partial x^2} = -\rho\,. \qquad \ldots (7.6)$$

where ρ *is the net charge density and* φ *is the electrostatic potential.*

The net charge density is calculated from the distribution function

$$\rho(x,t) = \sum q \int f(x,v,t)dV\,. \qquad \ldots (7.7)$$

As we are considering super particles for the system, the distribution function for electron is given by superposition of several elements

$$f(x,v,t) = \sum_p f_p(x,v,t)\,. \qquad \ldots (7.8)$$

f_p *is the distribution function of each super particles.*

Now we define each super particle with a special shape function according to their distribution.

$$f_p(x,v,t) = N_p S_x\left(x - x_p(t)\right) S_v\left(v - v_p(t)\right), \quad \ldots (7.9)$$

where $S_x \; and \; S_v$ are shape functions for position and velocity distribution of each super particle. And N_p is the number of particles present in the super particle.

Now let's define the shape function $S_x \; and \; S_v$ which essentially determines the super particle behaviour. The shape in the velocity direction as a Dirac's delta:

$$S_v\left(v - v_p(t)\right) = \delta\left(v - v_p(t)\right). \quad \ldots (7.10)$$

This is chosen so that the velocity of each particle in a super particle group has same velocity, so they remain in phase and no collision takes place within a super particle group. And for the spatial shape function, we use "b-spline" function. The b-spline functions are a series of consecutive higher order functions obtained from each other by successive integration.

The b-spline function is defined as $b_0(x) = \begin{cases} 1, & for\ |x| < \frac{1}{2} \\ 0, & otherwise \end{cases}$ ... (7.11)

And the subsequent b-splines are defined as $b_i(x) = \int_{-\infty}^{\infty} b_0(x - x')b_{i-1}(x')$ ... (7.12)

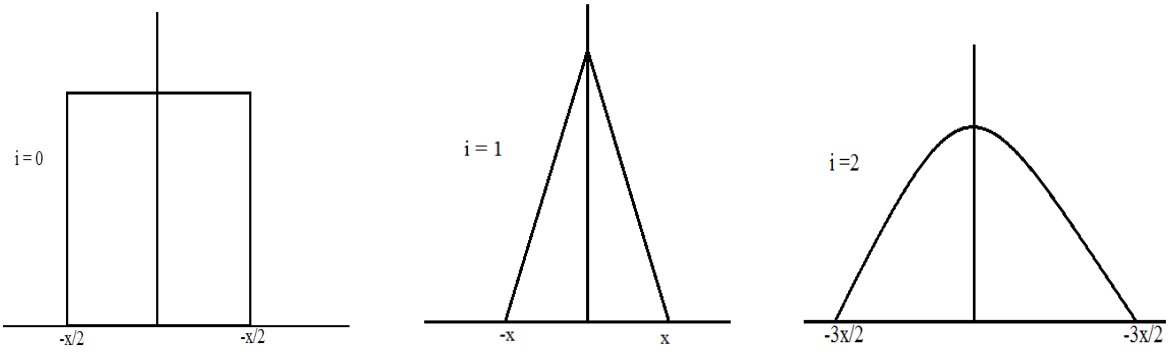

(a) (b) (c)

Fig 7.3 First 3 b-spline functions

Based on the b-spline function, the spatial shape function is chosen as

$$S_x(x - x_p) = b_i\left(\frac{x - x_p}{\Delta_p}\right), \quad \ldots (7.13)$$

where $\Delta_p \; is \; the \; scale \; length \; of \; the \; support \; of \; the \; super \; particle.$

Almost all PIC codes use splines of Zeroth order, very few use first order spline, because the particle is a uniform square cloud in phase space with infinitesimal span in the velocity direction and a finite size in space.

The linear superposition of all the super particles gives the total distribution function and if each super particle satisfies the Vlasov equation, the superposition does too. The electric field really depends on $f(x,v,t)$ making the Vlasov equation non-linear. As a consequence the electric field used in each Vlasov equation for each super particle must be the total electric field due to all super particles, the same entering the complete Vlasov equation. The electric field is itself given by Maxwell's equations which in turn need the charge density. The particle in cell approach described above provides immediately the charge density as the integral over the velocity variable of the distribution function, as described by equation 7.7. By combining equation 7.7, 7.8 and 7.9, we obtain:

$$\rho(x,t) = \sum_p qN_p S_x\left(x - x_p(t)\right). \quad \ldots(7.14)$$

To solve the field equation to obtain the electric field, we use a finite volume approach. Assuming the finite volume approach, a grid of equal cells of size Δx is introduced with cell centres x_i and cell vertices $x_{i+1/2}$. The scalar potential is discretized by introducing the cell-averaged values φ_i. The discrete form of the field equation is obtained by taking the second derivative in 1D with a corresponding discretized operator. The classic 3-point formula describes the Poisson's equation as:

$$\varepsilon_0 \frac{\varphi_{i+1} - 2\varphi_i + \varphi_{i-1}}{\Delta x^2} = \rho_i \ . \quad \ldots(7.15)$$

Defining the density as average over cells:

$$\rho_i = \frac{1}{x_{i+1/2} - x_{i-1/2}} \int_{x_{i-1/2}}^{x_{i+1/2}} \rho(x)dx \ , \quad \ldots(7.16)$$

$$\rho_i = \int_{x_{i-1/2}}^{x_{i+1/2}} \frac{\rho(x)}{\Delta x} dx \ , \quad \ldots(7.17)$$

where $\Delta x = x_{i+1/2} - x_{i-1/2}$.

By using the b-spline function, the density averaged over cell can be written as

$$\int_{x_{i-1/2}}^{x_{i+1/2}} \rho(x)dx = \int_{-\infty}^{\infty} b_0\left(\frac{x - x_i}{\Delta x}\right)\rho(x)dx. \quad \ldots(7.18)$$

Value of charge density can be obtained from equation 7.14 and putting in equation 7.17, we get:

$$\int_{x_{i-1/2}}^{x_{i+1/2}} \rho(x)dx = Q\sum_p \int_{-\infty}^{\infty} b_0\left(\frac{x - x_i}{\Delta x}\right) S_x\left(x - x_p\right)dx \ , \quad \ldots(7.19)$$

where $Q = qN_p$.

Now to compute the average cell density, we use an interpolation function for Zeroth order b-spline:

$$W(x_i - x_p) = \int S_x(x - x_p) b_0\left(\frac{x - x_i}{\Delta x}\right). \quad \ldots(7.20)$$

For higher order b-spline, the interpolation function is as follows:

$$W(x_i - x_p) = b_{i+1}\left(\frac{x_{i-}x_p}{\Delta x}\right).$$

After using the interpolation formula, the equation 7.19 becomes:

$$\int_{x_{i-1/2}}^{x_{i+1/2}} \rho(x)dx = Q\sum_p W(x_i - x_p) \quad \ldots(7.21)$$

Now the average cell density becomes:

$$\rho_i = \sum_p \frac{Q}{\Delta x} W(x_i - x_p). \quad \ldots(7.22)$$

Now the average charge density of each cell is known and putting this value in Poisson's equation 7.15, we obtain the potential of each cell φ_i. To compute the total fields acting on the particles in each cell, through a centred difference formula:

$$E_i = -\frac{\varphi_{i+1} - \varphi_{i-1}}{\Delta x}. \quad \ldots(7.23)$$

Assuming the field is constant in each cell and equal to the cell averaged value E_i , the total field acting on each cell is

$$E(x) = \sum_i E_i b_0\left(\frac{x - x_i}{\Delta x}\right). \quad \ldots(7.24)$$

Now the total electric field on each super particle can be defined as

$$E_p = \int S_x(x - x_p) E(x)dx.$$

$$E_p = \sum_i E_i \int b_0\left(\frac{x - x_i}{\Delta x}\right) S_x(x - x_p) \quad \ldots(7.25)$$

$$E_p = \sum_i E_i W(x_i - x_p), \quad \ldots(7.26)$$

Equation 7.26 gives the total electric field on each super particle in a 1D electrostatic PIC model. And the force on each super particle is given by

$$F(x_p) = q\int S(x - x_p)\, E_p(x_p)dx_p \quad \ldots(7.27)$$

7.3 ADVANCING THE PARTICLE

The equation of motion for particle p is

$$\frac{dv_p}{dt} = \frac{F(x_p,t)}{m_p} + \frac{q_p}{m_p c}\left(v_p \times B_0\right), \quad \ldots(7.28)$$

$$\frac{dx_p}{dt} = v_p(t)\ , \quad \ldots(7.29)$$

where $F\left(x_p,t\right)$ is the average force on each super particle given by equation 7.27. B_0 is the uniform external magnetic field. We advance $x_p\ and\ v_p$ using standard leap frog s algorithm [46]. The velocities are given at integer time step while positions are given at half-integer time step. The force depends on position and known at half integer time step. To compute the magnetic field we use average of velocity.

$$B_0 = \frac{{v_p}^{n+1} + {v_p}^{n}}{2} \quad \ldots(7.30)$$

Now the equation 7.28 can be written as

$$\frac{{v_p}^{n+1} - {v_p}^{n}}{\Delta t} = \frac{{F_p}^{n+\frac{1}{2}}}{m_p} + \frac{{v_p}^{n+1} + {v_p}^{n}}{2} \times \omega_{cp} \quad \ldots(7.31)$$

$$\frac{{x_p}^{n+\frac{1}{2}} - {x_p}^{n-\frac{1}{2}}}{\Delta t} = {v_p}^{n} \quad \ldots(7.32)$$

$\omega_{cp}\ is\ the\ electron\ cyclotron\ frequency\left(=\frac{q_p B_0}{m_p c}\right)$

The equation 7.31 transforms into

$${v_p}^{n+1} - {v_p}^{n+1} \times \frac{\omega_{cp}\Delta t}{2} = ({v_p}^{n} + {v_p}^{n} \times \frac{\omega_{cp}\Delta t}{2}) + \frac{{F_p}^{n+\frac{1}{2}}}{m_p}\Delta t \quad \ldots(7.33)$$

$${v_p}^{n+1}\ R\left[-\theta_{cp}\left(\frac{\Delta t}{2}\right)\right] = {v_p}^{n}\ R\left[\theta_{cp}\left(\frac{\Delta t}{2}\right)\right] + \frac{{F_p}^{n+\frac{1}{2}}}{m_p}\Delta t \quad \ldots(7.34)$$

where $R\left[\theta_{cp}\left(\frac{\Delta t}{2}\right)\right]$ is the rotational matrix for an angle $\theta_{cp}\left(\frac{\Delta t}{2}\right)$ about the magnetic field B_0.

As B_0 is in Z-direction. The rotational matrix will be as follows:

$$R\left[\theta_{cp}\left(\frac{\Delta t}{2}\right)\right] = \begin{bmatrix} Cos\left[\theta_{cp}\left(\frac{\Delta t}{2}\right)\right] & -Sin\left[\theta_{cp}\left(\frac{\Delta t}{2}\right)\right] & 0 \\ Sin\left[\theta_{cp}\left(\frac{\Delta t}{2}\right)\right] & Cos\left[\theta_{cp}\left(\frac{\Delta t}{2}\right)\right] & 0 \\ 0 & 0 & 1 \end{bmatrix}$$

Another property of Rotational matrix is $R\left[-\theta_{cp}\left(\frac{\Delta t}{2}\right)\right]^{-1} = R\left[\theta_{cp}\left(\frac{\Delta t}{2}\right)\right]$

From the equation 7.34

$$v_p{}^{n+1} = v_p{}^{n}\, R\left[\theta_{cp}(\Delta t)\right] + \frac{F_p{}^{n+\frac{1}{2}}}{m_p}\Delta t\, R\left[\theta_{cp}\left(\frac{\Delta t}{2}\right)\right] \quad \ldots(7.35)$$

New velocity is obtained from the old one by rotating it through an angle $\theta_{cp}(\Delta t)$ about the magnetic field and adding to it the change in velocity due to the electric field rotated through an angle $\theta_{cp}\left(\frac{\Delta t}{2}\right)$. In 1D limit the rotational matrix $R\left[\theta_{cp}(\Delta t)\right] = R\left[\theta_{cp}\left(\frac{\Delta t}{2}\right)\right] = 1$.

As we are considering 1D electrostatic model, the equation 7.35 transforms into:

$$v_p{}^{n+1} = v_p{}^{n} + \frac{F_p{}^{n+\frac{1}{2}}}{m_p}\Delta t \quad \ldots(7.36)$$

And the new position is given by the following:

$$x_p{}^{n+\frac{1}{2}} = x_p{}^{n-\frac{1}{2}} + v_p{}^{n}\,\Delta t \quad \ldots(7.37)$$

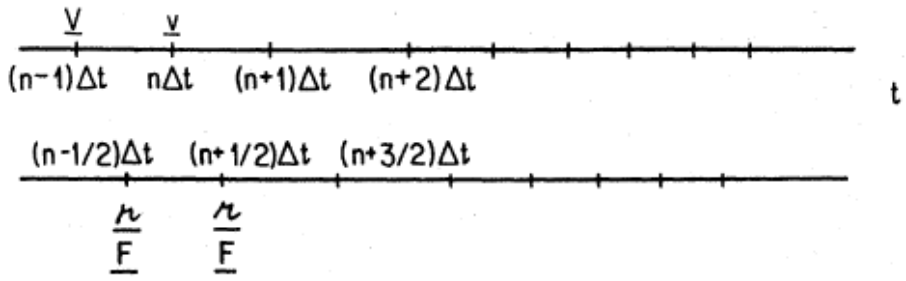

Fig.7.4 the Leap-frog algorithm

7.4 ALGORITHM OF PIC METHOD

STEP 1: Plasma is defined as a number of super particles having position x_p and velocity v_p each consisting of N_p number of physical particle.

STEP 2: The equations of motion for particles are advanced by one time step using particle electric field from previous time step.

$$x_p{}^{n+\frac{1}{2}} = x_p{}^{n-\frac{1}{2}} + v_p{}^{n}\,\Delta t$$

$$v_p{}^{n+1} = v_p{}^{n} + \frac{F_p{}^{n+\frac{1}{2}}}{m_p}\Delta t$$

STEP 3: The charge densities are computed in each cell using

$$\rho_i = \sum_p \frac{Q}{\Delta x} W(x_i - x_p)$$

STEP 4: The Poisson's equation is solved using

$$\varepsilon_0 \frac{\varphi_{i+1} - 2\varphi_i + \varphi_{i-1}}{\Delta x^2} = \rho_i$$

And the electric field E_i in each cell is computed through

$$E_i = -\frac{\varphi_{i+1} - \varphi_{i-1}}{\Delta x}$$

STEP 5: from the field known in the cells, the field acting on the particles is computed as

$$E_p = \sum_i E_i W(x_i - x_p)$$

This is used in next cycle.

STEP 6: Repeat the cycle.

The first thing to consider in running a PIC code is a proper choice of the time step and of the grid spacing. The time step needs to resolve both light-wave propagation and Langmuir wave propagation:

$$c\Delta t < \Delta x \quad \ldots (7.38)$$

$$\omega_{pe}\Delta t < 2 \quad \ldots (7.39)$$

The grid spacing needs to resolve the electron Debye length to avoid the so-called finite grid instability due to the aliasing of different Fourier modes:

$$\Delta x < \varsigma \lambda_D \quad \ldots (7.40)$$

where ς is a constant order of 1 whose exact value depends upon the choice of interpolation and assignment function.

The PIC method conserves momentum but not energy. The fundamental reason is that in practice the PIC method uses many particles per cell: there are infinite particle configurations resulting in the same value of the quantities projected to the grid. This degree of freedom is what causes the finite grid instability and the lack of so, the energy needs to be monitored and the time step and grid spacing need to be chosen sufficiently small as to conserve energy. Usually the time step has to be less than 1/10 of its stability limit and the grid spacing less than 1/3 for energy to be conserved sufficiently.

7.5 VORPAL CODE

All simulations presented in this paper are done through VORPAL codes. Details about this code can be found on their website [3]. It is a relativistic, arbitrary dimensional, hybrid plasma and beam simulation code. The kinetic plasma model incorporated in VORPAL is based on the particle-in-cell (PIC) algorithm, both in the electromagnetic and electrostatic limits. In the electrostatic limit, VORPAL solves Poisson's equation at every time step based on the instantaneous charge distribution. In the electromagnetic limit, a charge-conserving current deposition algorithm enables the integration of Maxwell's equations without any additional divergence correction.

The plasma can be confined in arbitrarily shaped structures for particles and fields, including conductors, particle absorbers, reflectors, and many more. In both electrostatic and electromagnetic simulations, the computational domain can be periodic or mimic boundaries at infinity via perfectly matched layer (PML) boundary conditions.

VorpalComposer provides an interface that allows you to edit and validate your simulation input files, run VORPAL simulations, and visualize results using the VisIt-based VorpalComposer Visualization tool.

CHAPTER VIII

8. SIMULATIONS AND RESULTS

All simulations presented here are done on VORPAL and the outputs are solved using a python program. The main aim of the simulations is electron acceleration in the bubble regime and optimization of the energy gain in the bubble regime of the LWFA.

8.1 SIMULATION OVERVIEW

As described in section 6.3, in this work I have used an upward density ramp technique to optimize the energy gain. A plasma density ramp was easily generated by using the supersonic gas nozzle. The structure of density ramp is as shown below

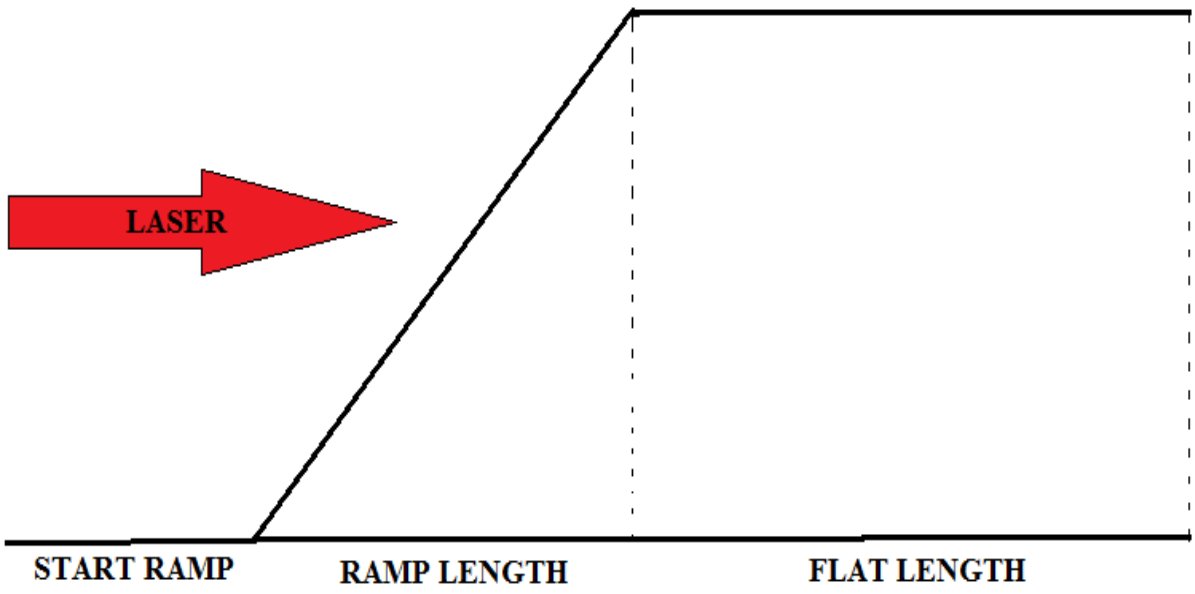

Fig.8.1 Simulation Density structure

As shown in the Fig.8.1 the plasma consists of a uniform plasma density preceded by an upward density ramp. The vacuum space (start ramp) at the start of the plasma is provided to take care of experimental environment. The plasma should be started in such a way that the

Laser at the start is completely absorbed by the plasma particles. If vacuum space is not provided at start, the mesh will start moving on its course, but plasma is not loaded at that point.

The laser is launched at x=0 and focused at the middle of the ramp, what we called in our simulation as the laser "waist position". First the electron acceleration is simulated for a uniform plasma density with no upward density ramp. Then the ramp length was varied for different simulation and results were compared. And as according to the theory, the energy of the output beam increased as our ramp length increased.

The laser parameters are kept unchanged for all the simulations except for the scaling laws comparison. We have used an X-polarized Gaussian laser pulse profile of

$$a = a_0 \exp\left(\frac{-r^2}{{r_0}^2}\right) \cos(kx - \omega t)\, \hat{x}$$

The simulation is Vorpal is divided into 3 parts, (i) create input file (ii) Run Vorpal (iii) Visualize the data. The simulation domain size was chosen such that several RMS intensity pulse lengths and laser pulse lengths are continuously in the domain. The simulation time is set to run until shortly after the pulse leaves the plasma. For the grid spacing, the longitudinal size was determined based on the necessity to resolve the laser wavelength. A Gaussian pulse wave launcher is set as a boundary condition on the z component of the electric field which is launched into an electron species with a density ramp into a uniform species density. The moving window allows for a smaller simulation domain while still allowing the laser pulse to propagate further into the plasma as time increases.

8.2 CREATING THE INPUT FILE

A VORPAL input file contains a hierarchical set of code blocks and variables that describe the structure and behavior of a simulation model. To define the simulation, you first create an input file. There are actually two types of input file formats: the format that is input to the pre-processor (has the suffix .pre) and the format that is input to VORPAL (has the suffix .in). The main difference between the formats is that pre file code has not yet been translated to contain actual values in place of symbols. Using symbols instead of actual values allows you to use the same input file for multiple simulations, therefore all the parameters are inputted through a pre file in VorpalComposer. Details are provided in Appendix 1.

8.3 OPTIMIZATION OF ENERGY GAIN

The laser parameters are kept constant at a_0=4.0, spot size (r_0) =8.5µm, laser power (P) =10 Tera-watt, Laser pulse duration (τ) =55fs, laser wavelength (λ) =0.8µm, L_{rms}=7µm, and as we use a Gaussian pulse; k_p L_{rms}=1

For all the four simulations performed. Particles per cell is considered as 1. The number of cells on X-axis depends on the value of L_{rms}, while number of cells on Y-axis depends on the spot size of laser. The number of cells on X-axis and Y-axis are 3939 and 256, and each cell has a spacing of 2.67×10^{-8} m in X-axis and 2.0×10^{-7} m in Y-axis. As we are performing all our simulations in 2D, all the Z-axis parameters are not considered. The nominal plasma density is 4×10^{25} m^{-3}.

SIMULATION 1:

Simulation 1 is run with a uniform plasma density of 4×10^{25} m^{-3} for a length of 1000µm. As from our data, the bubble is visible after the laser travels a length of ~350µm in the plasma, shown in Fig 8.2.

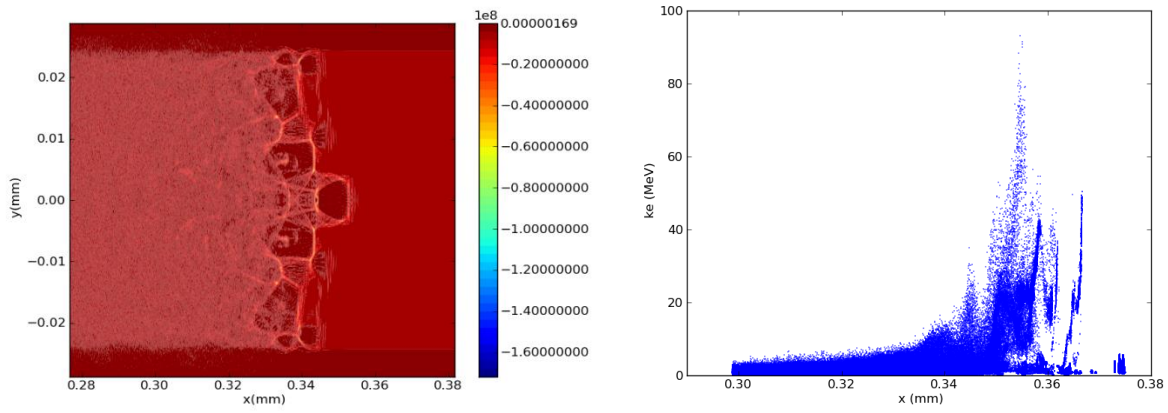

(a) (b)

Fig.8.2 Simulation 1 (Time step=1.26ps): Plasma Bubble formation at ~350µm at (a) Plasma density contour showing the bubble formation (b) Kinetic energy plot of plasma electron

Fig.8.3 shows the plasma density variation and plot of electron energy (MeV) with the plasma length at the position where electrons have gained maximum energy. As the visualization shows the maximum energy gained by the electrons is 200MeV at 620µm, after the laser travels

for 2.23ps and beyond that, the energy starts to decrease, as the electrons decelerate due to dephasing and pump depletion.

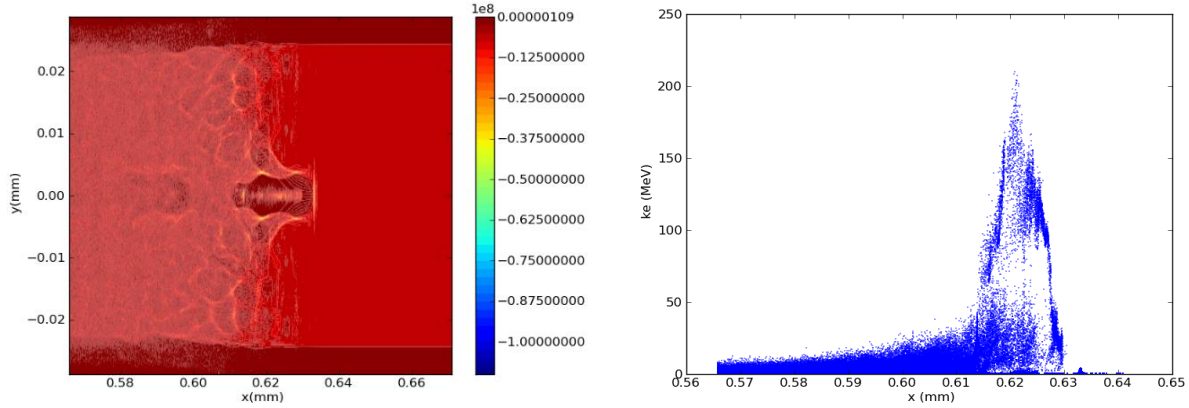

(a) (b)

Fig.8.3 Simulation 1: (Time step=2.23ps) (a) Plasma density contour at maximum energy (b) Kinetic energy plot of plasma electrons at maximum energy position

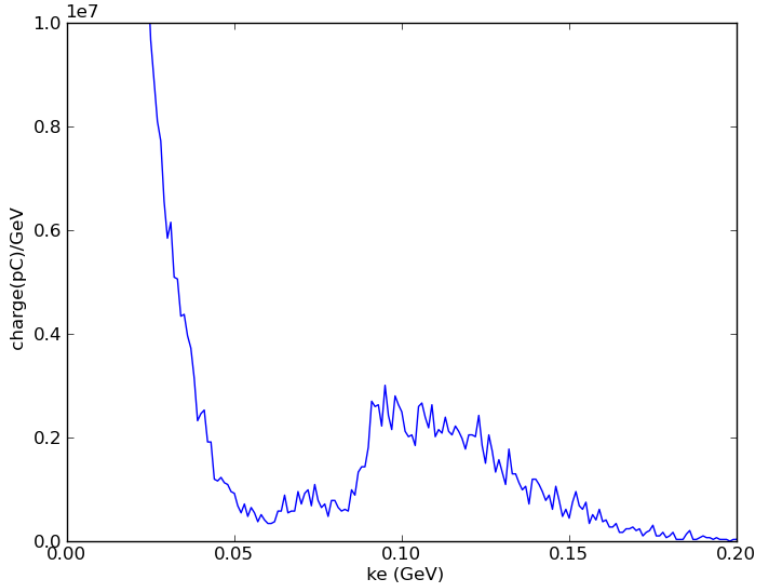

Fig.8.4 Simulation 1: Histogram plot of plasma electrons at 2.23ps

As the Fig.8.4 shows the accelerated electron bunch has most particles around 100-120MeV, very few particles has the maximum energy of 200MeV. And as the laser travels further, the energy spread of the accelerated bunch increases.

Using the expression for Maximum energy gain by electron (ΔW) from Table 6.1, as our laser envelope is in non-linear limit, the acceleration length will be limited by pump depletion

rather than dephasing. So the expression for ΔW in non-linear regime with pump depletion limitation,

$$\Delta W(MeV) \approx \frac{400\, I\left(\frac{W}{cm^2}\right)}{n(cm^{-3})} \quad \ldots (8.1)$$

After using our input laser parameter value and plasma density, this yields the maximum energy gain value as 85.6MeV (E_{theory}), which is almost equal to our simulation value of ~100MeV (E_{sim}).

As it is explained in chapter VI, that the acceleration length will be limited by the pump depletion in this simulation as our laser is in non-linear limit. So now let's calculate the pump depletion length and compare it with the simulation result.

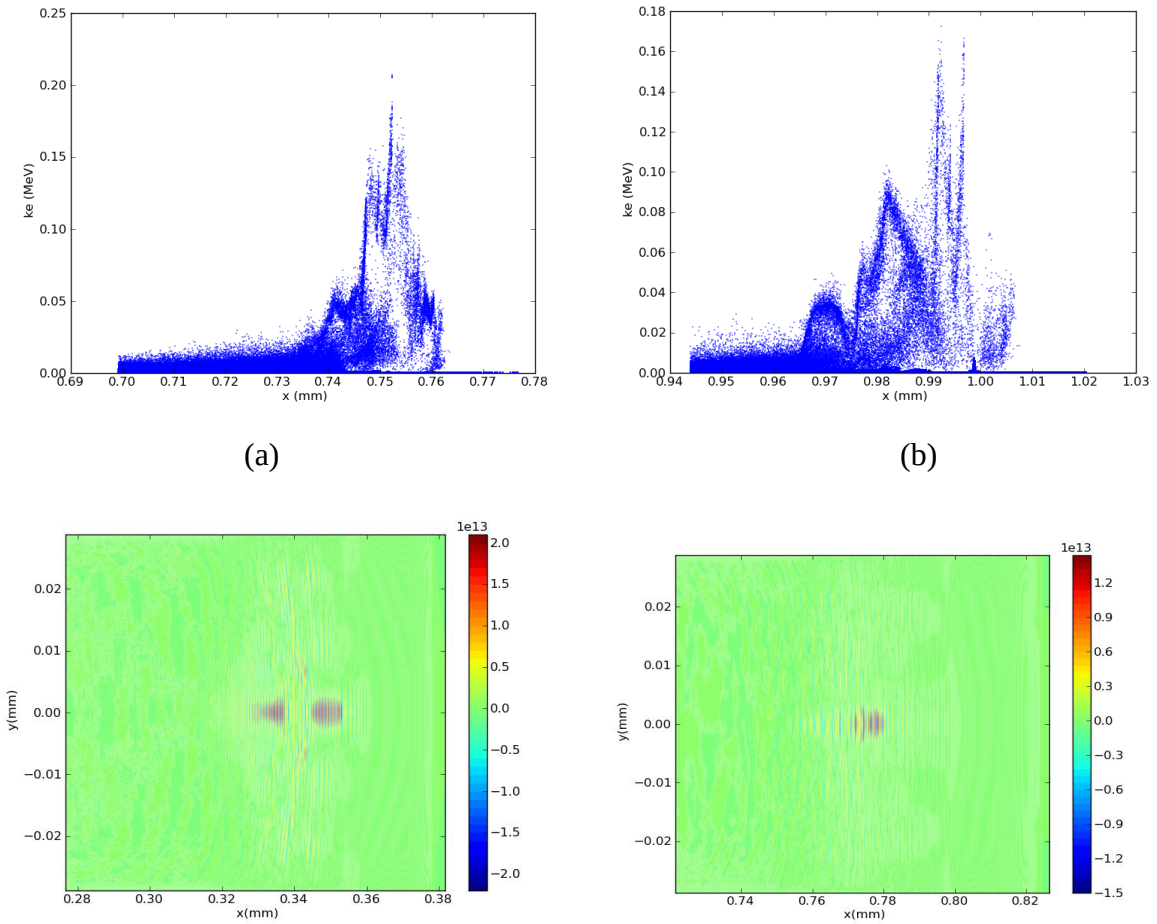

Fig.8.5 Simulation 1: Kinetic energy plot of plasma electrons during depletion at time step of (a) 2.76ps (b) 3.5ps (c) Laser electric field plot at 1.26ps (d) Laser field plot at 2.76ps

From Fig.8.5, we can see that as the laser travels further the energy peak is decreasing and also the energy spread is also increasing, which reduces the output beam quality. The depletion of laser can be seen from fig 8.5 (c) and (d). From the simulation, I have observed that, the bubble forms at 350µm, and the pump depletes at ~750µm. So the depletion length will be around ~400µm ($L_{pd(sim)}$).

According to the equation 6.2, the expression for non-linear depletion length is

$$L_{pd(theory)} = \frac{\lambda_p^3}{\lambda^2} \times \frac{\sqrt{2}}{\pi} a_0 = 414.139\mu m$$

SIMULATION 2:

Simulation 2 is run with a plasma ramp length of 300µm and succeeded by a flat length of 700 µm. All other parameters are kept same as simulation 1. As per the Vorpal output the bubble forms at ~470µm.

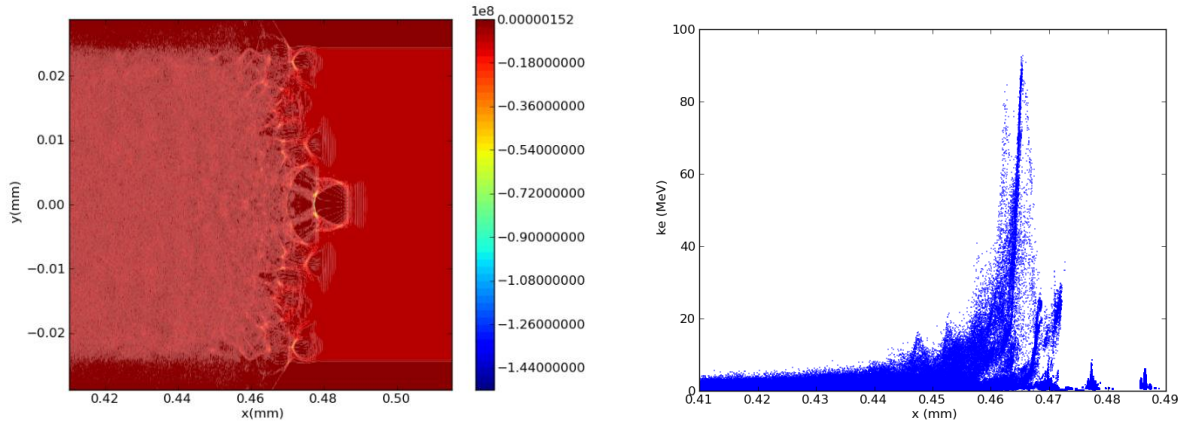

(a) (b)

Fig.8.6 simulation 2 (Time step=1.71ps): (a) Plasma density contour during bubble formation (b) Kinetic energy plot of plasma electrons

From the figure 8.6 it can be seen that, the bubble formation starts at 470µm and plasma electrons achieve the maximum energy of ~200 MeV at 735µm after which the energy of plasma electrons start to decrease.

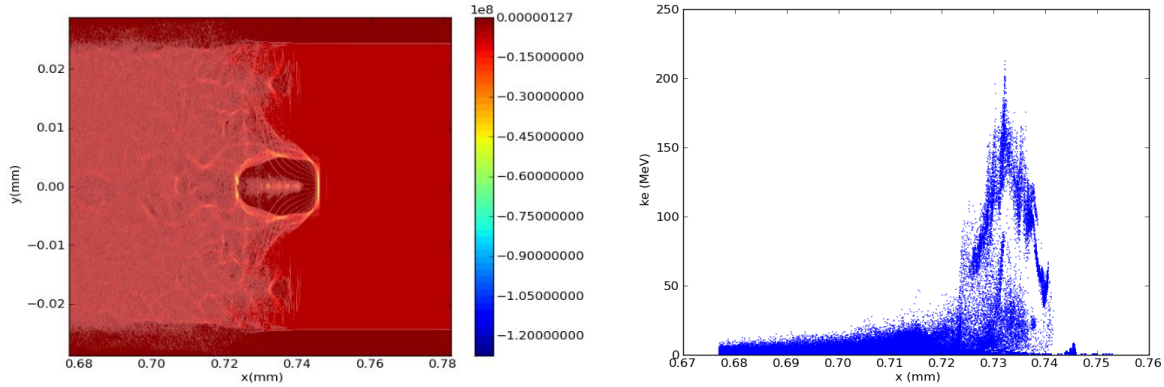

(a) (b)

Fig 8.7 Simulation 2 (Time step=2.6ps): (a) Plasma density contour at maximum energy (b) Kinetic energy plot of plasma electrons.

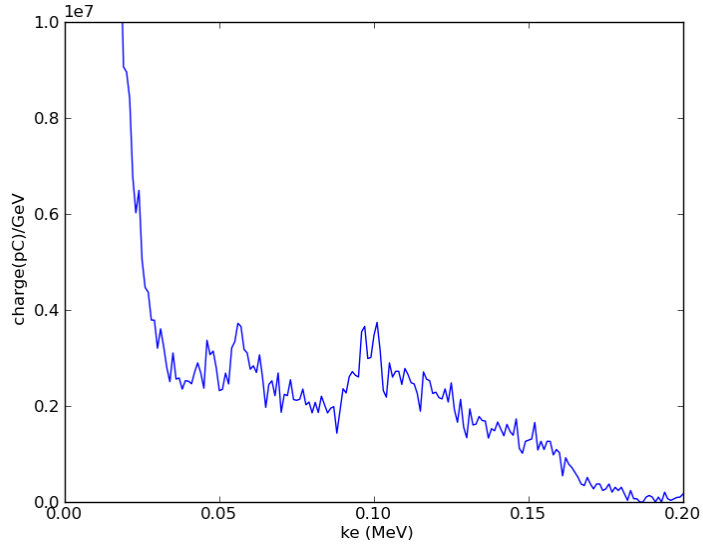

Fig.8.8 Simulation 2: Histogram plot of plasma electrons at 2.6ps

As the Fig.8.6 shows the accelerated electron bunch has most particles around 100-120MeV, very few particles has the maximum energy of 200MeV. And as the laser travels further, the energy spread of the accelerated bunch increases.

Any theoretical estimation is not available for the plasma density structure of simulation 2, unlike simulation 1, where the density is uniform throughout the plasma length, so as the plasma wavelength undergoes a uniform change due to laser which can be estimated or expressions has been already derived for uniform plasma density structure. But in simulation 2 a density ramp is inserted before the flat length, which causes the plasma wavelength to increase

non-linearly. So the $L_{pd} \propto \lambda_p^3$ increases and so as the $\Delta W \propto L_{acc} = \frac{L_{pd}}{2}$ will increase, and the simulation results proves the same. The laser depletion and its effect on energy gain can be observed from Fig.8.9. From simulation, the depletion length is calculated to be ~430 µm.

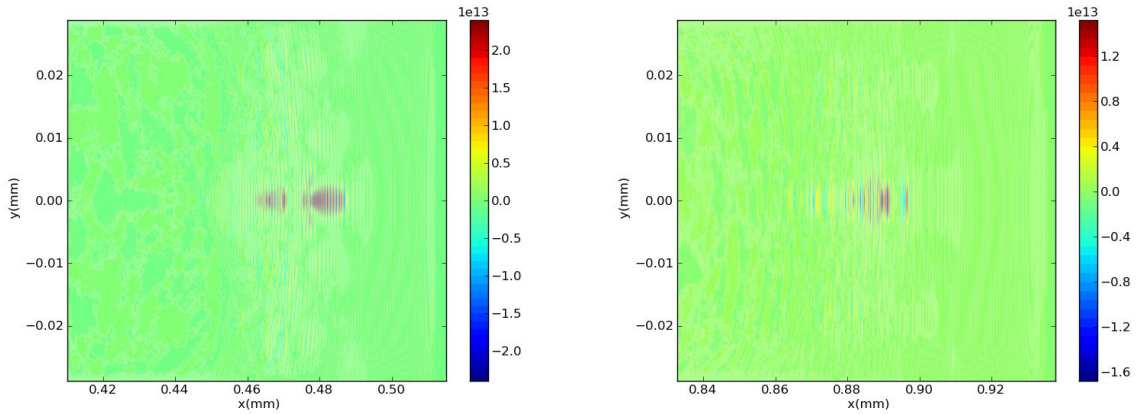

(a) (b)

Fig.8.9 Laser electric field plot at (a) Formation of bubble time step=1.71ps (b) depletion of laser Time step=3.11ps

SIMULATION 3:

Simulation 3 is run with a laser propagating through a plasma density ramp length of 500µm succeeded by a flat length of 1000 µm. All other parameters are kept constant. As per the Vorpal output the bubble forms at ~600µm.

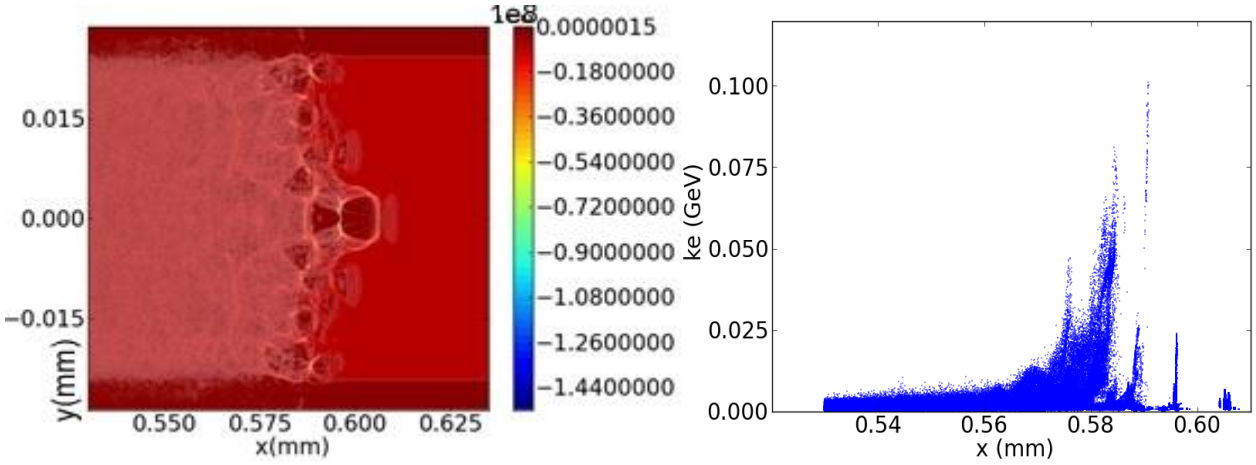

(a) (b)

Fig.8.10 Simulation 3: (Time step=2.15ps) (a) Plasma bubble forms at ~600µm (b) Kinetic Energy plot of plasma electrons

As the fig.8.11 shows the maximum energy of ~320MeV is achieved by the plasma electrons at 950µm after which the energy of plasma electrons start to decrease.

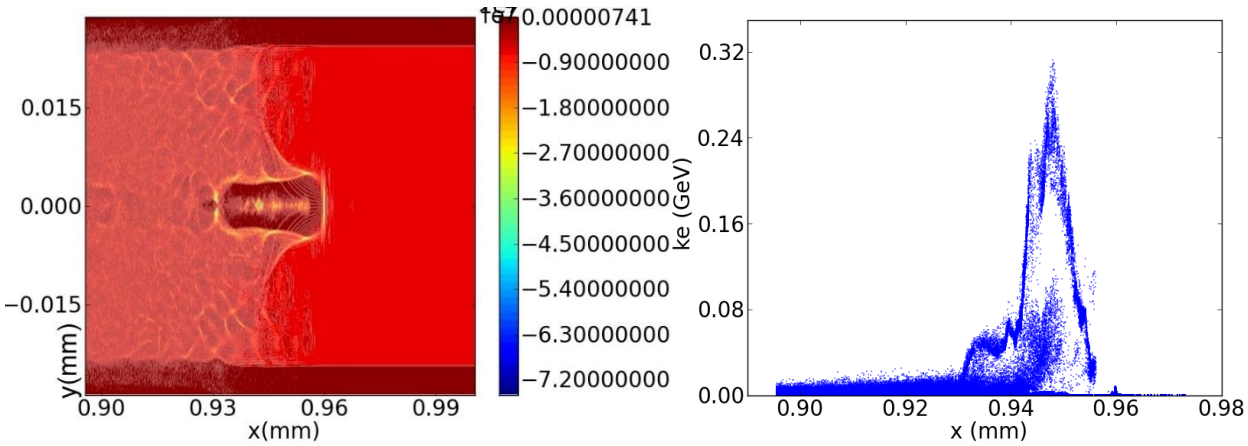

(a) (b)

Fig.8.11 Simulation 3 (Tim step=3.27 ps): (a) Plasma density contour at maximum energy (b) Kinetic energy plot of plasma electrons at Maximum energy

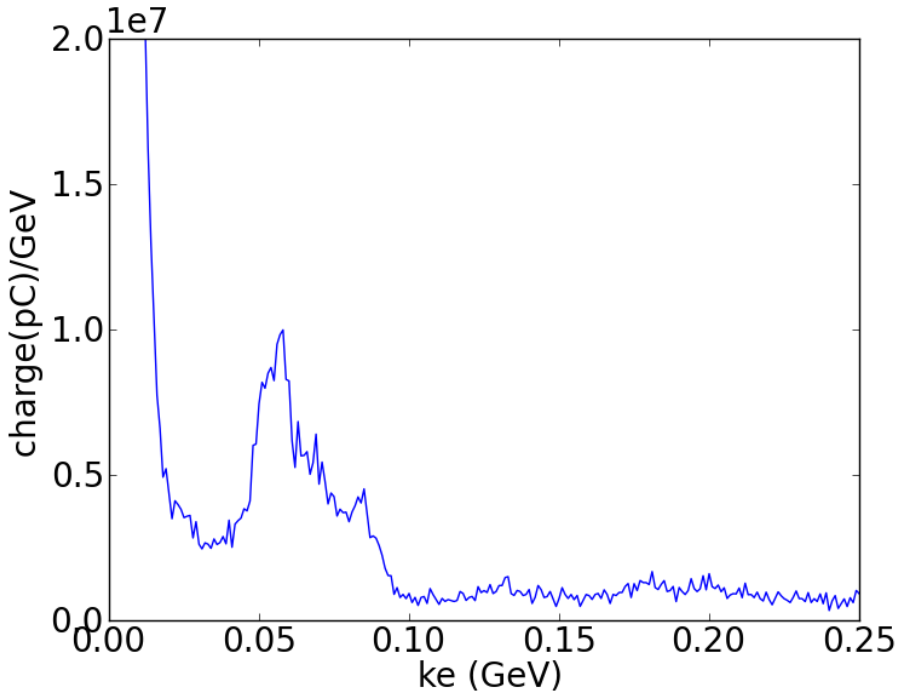

Fig.8.12 Simulation 3: Histogram plot of plasma electrons at 2.6pS

As the fig.8.12 shows maximum charge is collected at 50-100MeV energy, but this energy is too low for our consideration. The energy of electrons ranged up to 320MeV. Laser pump depletion can be seen from fig.8.13. The pump depletion length can be calculated as ~480µm.

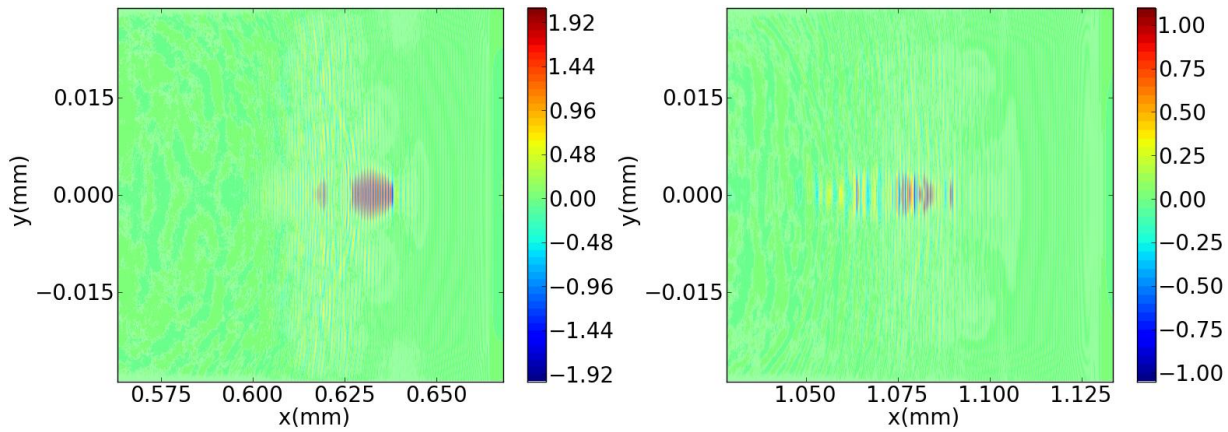

Fig.8.13 Simulation 3: Laser electric field (a) 2.15 ps (b) 3.27 ps

SIMULATION 4:

The 4th Simulation is run with a laser propagating through a plasma density ramp length of 700µm succeeded by a flat length of 800 µm. All other parameters are kept constant. As per the Vorpal output the bubble forms at ~720µm.

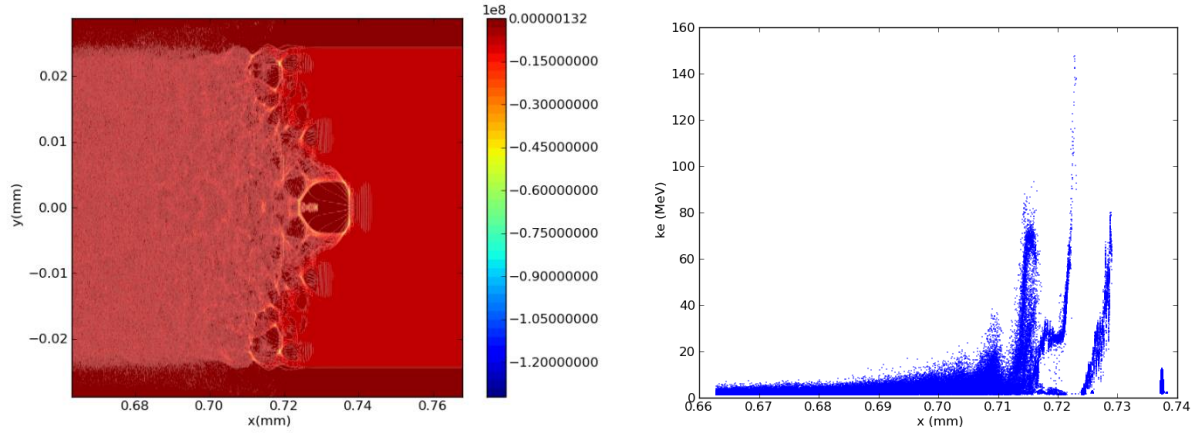

(a) (b)

Fig.8.14 Simulation 4: (Time step=2.5ps) (a) Plasma bubble formation at 720µm (b) Kinetic Energy plots of Plasma electrons at bubble formation

Plasma electrons achieve maximum energy of more than 300 MeV at 1005µm, after which the second injection electrons dominate the kinetic energy plot and plasma electrons from the first injection starts to decrease due to pump depletion. The secondary injection is shown in fig.8.16.

The fig.8.16 (b) shows that maximum charge is collected at 50 MeV, but the energy of the electron at that charge is too low for our consideration, rather we consider the second peak at 250 MeV, although it has less charge and resolution compared to the first one, the electron energy is our consideration factor. The laser depletion occurs at 1350μm as shown in fig.8.17.

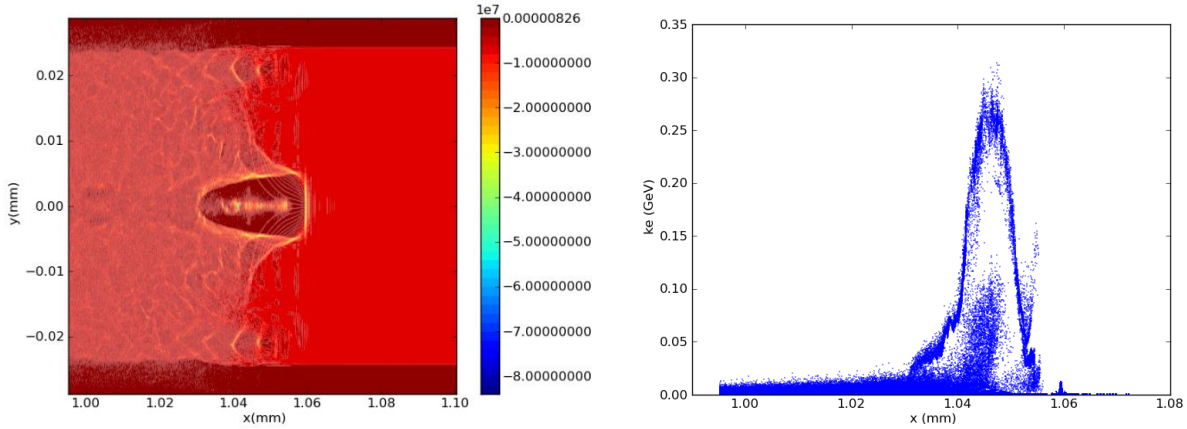

(a) (b)

Fig 8.15 Simulation 4: (Time step=3.6 ps) (a) Plasma density contour at maximum energy position (b) Kinetic energy Plot of plasma electrons at Maximum energy

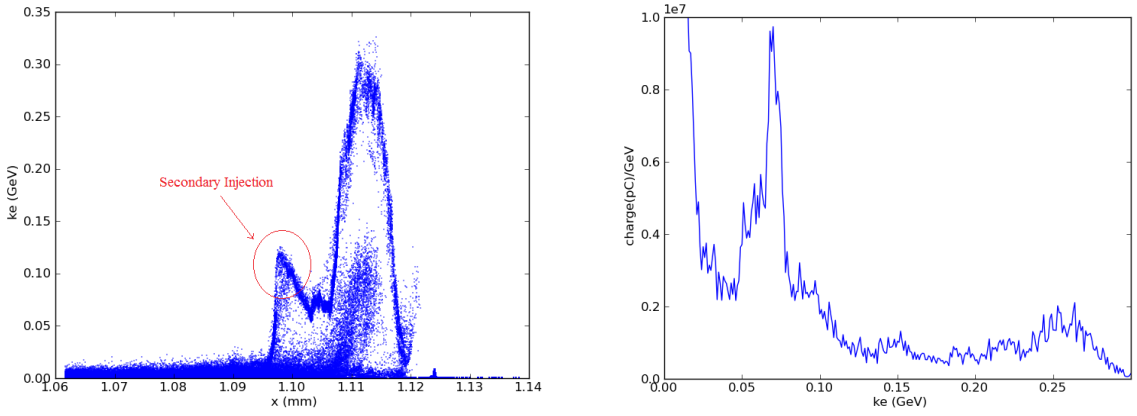

(a) (b)

Fig 8.16 Simulation 4: (a) Kinetic energy plot of plasma electrons shows Secondary injection takes place at Time step=3.8 ps and first injection energy spread and peak starts to decrease. (b)Histogram plot of plasma electron at 3.6 ps.

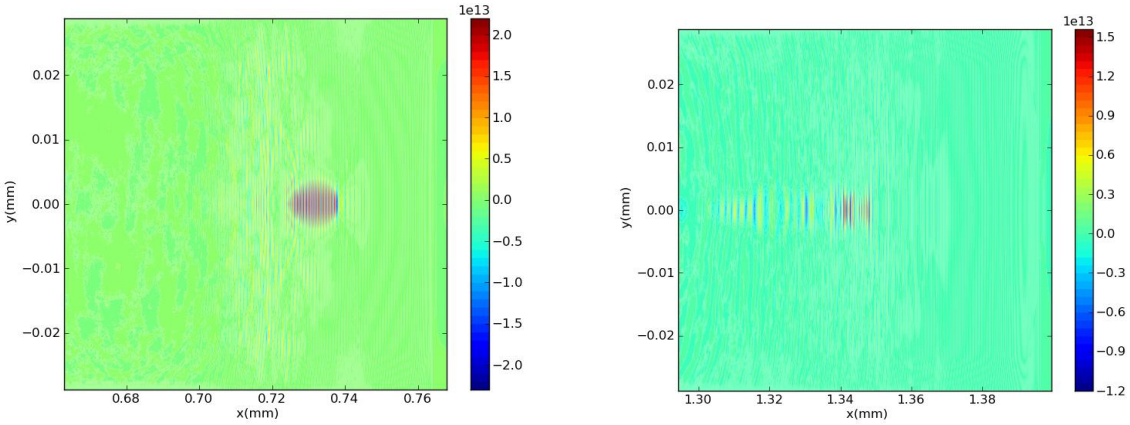

(a) (b)

Fig.8.17 Simulation 4: Laser electric field plot at (a) Time step= 2.5 ps (b) Time step=4.56 ps

From simulation, the depletion length is calculated to be around 630μm.

COMPARISION:

From the comparison of all the simulation, we can conclude following points.

(i) The radius of the bubble increases with the increase in ramp length. This implies that number of electrons trapped in the bubble also increases. Higher the number of electrons trapped inside the bubble, greater the charge collected by the output beam.

(ii) As the bubble radius increases, the focusing gradient or the radial electric field (eqn.5.15), which is directly proportional to the bubble radius also increases, hence our the resonance of the output beam will improve so as the emittance. The radial focusing force (Eqn.5.14), which is also directly proportional to the bubble radius, increases with the increase in the plasma density ramp length.

(iii) With increase in ramp length, the plasma density is constantly increasing. From Eqn.5.11, it can be seen that the accelerating gradient or the axial electric field, which is the primary reason for electron acceleration inside the bubble, is directly proportional to plasma density. So as the density is increasing constantly, the axial electric field is increasing and electrons inside the bubble experience a higher magnitude of accelerating force.

All three above points constitute the fact that the maximum energy gained by the electron will increase if we increase the ramp length of the plasma density profile. The simulation results

prove the same, as we can see, the 4th simulation which has the maximum ramp length (700μm) has the plasma electrons of maximum energy i.e. ~300MeV.

Also if we compare Fig.8.3 (b), 8.7(b), 8.11(b) and 8.15(b), we can see that the, resolution of the kinetic energy peak is getting better as the ramp length is increasing, which implies that the number of monoenergetic electrons are increasing. Thus our primary aim of optimizing the electron energy gain inside the bubble of a LWFA is achieved.

CHAPTER IX

9. FUTURE PROSPECTS AND APPLICATION

So far, in this experiment, I was only able to accelerate electrons to several 100-300MeV using the bubble regime. Higher energies can be achieved for but in a slightly different regime using beam guiding. According to scaling laws, energies of even GeV would be possible given strong enough lasers. The reason for the need of this high energies are dephasing and pulse depletion, as explained in the chapters 6.1 and 6.2. Since the energy of the laser pulse is depleted at some point and electrons start catching up with the laser pulse, bubble acceleration has a limited acceleration length. Another problem is the beam quality at high energies, the energy spread of the electrons increases at high laser amplitudes due to synchrotron radiation. Therefore the bunch of accelerated electrons has a wider range of velocities and would be less useful for example the application in a FEL than electrons created with smaller laser amplitudes.

9.1 EXTERNAL INJECTION

Another method to improve the beam quality is to inject the electrons to be externally. Electron motion during wave breaking is rather chaotic. Because of this, initial velocities and positions of electrons at the back side of the bubble tend to vary. Also, self-injection seems to be a process which does take place over a certain period of time. As can be seen in figure 5.2, electrons inside the bubble are spread over a certain area and, because of this, are subject to different field strengths. This of course leads to a certain spread in the energy histogram around the energy predicted by the theory. In order to reduce this energy spread, one possible way might be trying to avoid self-injection. Instead of self-injected electrons with their issues mentioned before, one could try to inject an electron beam with good beam quality into the bubble. If it would be possible to inject such a beam into a bubble, the resulting beam after the acceleration could have significantly improved properties over self-injected electron beams. However, slow, self-injected electrons would interfere with the faster injected electron beam. In order to keep slow electrons from affecting the acceleration by beam loading and other effects, self-injection should be avoided in this scheme. There are few methods of external electron injection e.g.

Ponderomotive Injection, Collider pulse injection scheme. In ponderomotive injection, two pulses are pumped perpendicular to each other, first pulse creates a Wakefield and Second Pulse (Injection pulse) intersects the pump pulse and the Ponderomotive force associated with it accelerates fraction of plasma electrons such that they get trapped in Wakefield. In colliding pulse injection method, the injection is due to Pondermotive force associated with Slow Beat wave of 2 intersecting pulses.

9.2 STAGING ACCELERATION

Using the idea of injecting accelerated electrons into an existing bubble, the next reasonable step seems to be staging acceleration. Depletion of a laser pulse as well as dephasing, limit the acceleration length of trapped electrons. Together with the acceleration length, the total energy gain is limited. In order to work around depletion and dephasing one possible solution might be to use several bubbles instead of just one. In one stage, the electrons of one bubble, after travelling their acceleration length, are extracted from the old bubble. In the next stage, the electrons are injected into a new bubble. One possible way of realizing staging acceleration would be to use oblique mirrors in order to separate each stage. A highly over-dense plasma would reflect the laser pulse driving the bubble. Electrons of high enough energy would have a very small cross-section for interaction with the mirror and therefore pass it with little to no effect.

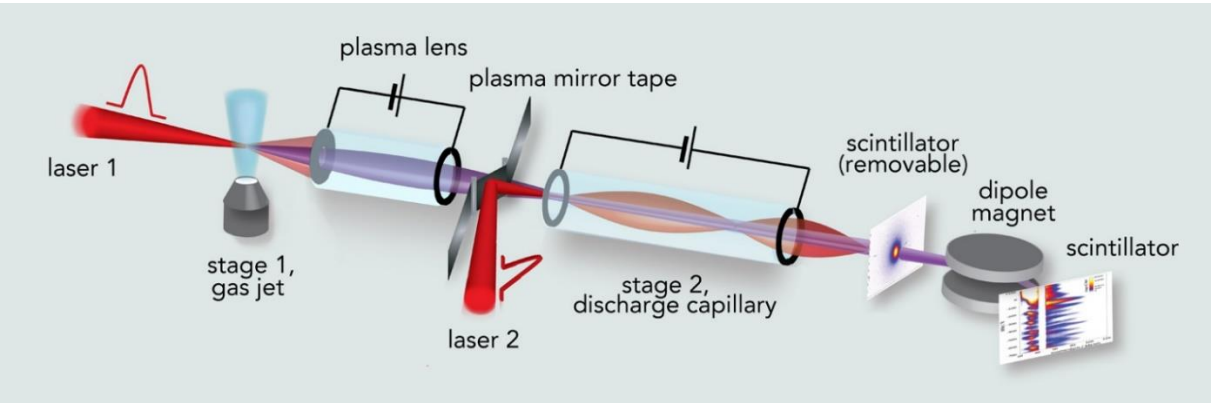

Fig.9.1 A two-staged laser plasma accelerator

(Coupling of 2 ‘Tabletop’ Laser-Plasma Accelerators, a Decisive First Step toward tomorrow’s Ultra powerful Compact Machines.) http://newscenter.lbl.gov/2016/02/01/2-stage-laser-plasma-accelerator

CHAPTER X

10. CONCLUSION

The main aim of this work is to optimize the energy gain of electrons inside the bubble regime using different plasma density structure. For this, four simulations have been conducted and results are compared to each other, and as well as to the theoretical prediction. The simulation results vary from our theoretical prediction by ~14%, due to the fact that, the simulations are conducted in 2D PIC method due to available memory constraint, while theoretical predictions are in 3D. In 2D the laser electric field energy is only dissipated in two dimension so more energy is available to the electrons for acceleration, while in 3D the laser electric field has one more extra degree of freedom, so losses are more in case of 3D. At very low spot sizes $r_0 \leq 2\lambda$ or very low laser amplitudes $a_0 \leq 4$, bubbles were not created clearly and observed energies did not match the predictions. Also if we increase the plasma density, higher laser power is needed for any considerable laser plasma interaction to take place. Also lots of other contributing factors are ignored to avoid complexity in simulation and calculation e.g. synchrotron radiation, Betatron oscillation. My work included several references, which made it possible to compare results from simulation to data gained from experimental studies and other simulations conducted. I was also able to confirm that simulations with the VORPAL code are able to reproduce electron energies very similar to ones obtained from data of corresponding experiments. The simulated electrons achieved slightly more energy and the histogram plots are little bit noisier. But the kinetic energy plots show a sharp monoenergetic beam, although the beam quality is not as expected, but within reasonable limits. All these errors could be eliminated by taking more practical parameters and three dimensional simulation. Even though laser plasma acceleration technique was developed since 1980s, but there are still plenty of areas those need to be investigated and perfected. The answer to the future of acceleration and high energy physics is laser plasma accelerators, those will replace the conventional accelerator as accelerating device in future due to requirement of higher energy particle and better beam resolution.

APPENDIX I

```
##########################################################################
# Defined parameters
# --------------------------------------------------------------------
# Physical constants

$ import mathphys.mac
$ CLASSICAL_E_RADIUS = ELEMCHARGE / (4 * PI * EPSILON0 * ELECMASSEV)
# --------------------------------------------------------------------
# Input file switches for possible command-line override
$ NDIM = 2
#====================================================================
# User-defined parameters
#====================================================================
# Plasma parameters
# Density in uniform region
$ DENSITY = 4.0e25
# Longitudinal profile parameters: The left edge of the simulation will be at x = 0, and the laser will be
launched from that point. Then STARTRAMP is the start of the plasma both in absolute coordinates and
relative to the laser launch surface.
$ STARTRAMP = 10.e-6
$ RAMPLEN = 0       #Change the value of ramp length for different simulations. RAMPLEN=0 for
uniform density
$ FLATLEN = 1000.e-6
# --------------------------------------------------------------------
# Laser parameters
$ WAVELENGTH = 0.8e-6
# Laser pulse length: This is the RMS of the intensity, so that
# intensity goes as I = I_0 * exp(-x^2 / 2L_RMS^2).  In units of m.
$ KP_LRMS = 1.
# Waist size, corresponding to standard Gaussian form I = I_0 *
# exp(-2r^2 / W_0^2)
$ W_0 = 8.5e-6
# Normalized vector potential
$ A_0 = 4.0
# --------------------------------------------------------------------
# Grid paramaters
$ N_LAMBDA_X = 30.
$ N_LAMBDA_T = 4.
# --------------------------------------------------------------------
# PML parameters
$ NPML = 16
$ PML_EXP = 4
$ SIGMA_FAC = 1.0
# --------------------------------------------------------------------
# Particles per cell
# 1 dimension
$ PPCX_1 = 4.
# 2 dimensions
```

```
$ PPCX_2 = 1.
$ PPCY_2 = 1.
# 3 dimensions
$ PPCX_3 = 1.
$ PPCY_3 = 1.
$ PPCZ_3 = 1.
# Algorithm parameters
$ CDTFAC = 0.9995
#=========================================================================
# Derived parameters
#=========================================================================
# ------------------------------------------------------------------------
# Derived plasma parameters
$ K_P = math.sqrt(4 * PI * DENSITY * CLASSICAL_E_RADIUS)
$ LAMBDA_P = TWOPI / K_P
# ------------------------------------------------------------------------
# Derived laser parameters
$ K_0 = TWOPI / WAVELENGTH
$ OMEGA = LIGHTSPEED * K_0
# RMS intensity pulse length
$ L_FWHM = LIGHTSPEED * 55E-15
# Pulse length: Full width at half max of intensity (not field)
$ L_RMS = L_FWHM / math.sqrt(8 * math.log(2.))
# VORPAL translation of transverse spot size
$ WYPUMP = W_0 * math.sqrt(2.)
$ WZPUMP = W_0 * math.sqrt(2.)
# Electric field peak amplitude
$ E_0 = A_0 * K_0 * ELECMASSEV
# ------------------------------------------------------------------------
# Plasma longitudinal profile
$ STARTFLAT = STARTRAMP + RAMPLEN
$ ENDFLAT = STARTFLAT + FLATLEN
$ ENDPLASMA = ENDFLAT
# ------------------------------------------------------------------------
# Laser position parameters
# The full half-witdh of the laser pulse, i.e. the length between the peak and where the truncated envelope
reaches 0.
$ L_HALF = 5 * L_RMS
# The position of the peak of the laser pulse at the beginning of the simulation (before it enters the global
domain)
$ XSTARTPUMP = -L_HALF
# Waist position, relative to launch surface at x = 0.  We focus in the middle of the ramp.
$ WAISTPOS = (STARTRAMP + STARTFLAT) / 2
# ------------------------------------------------------------------------
# Grid parameters
# Minimum global domain sizes.  Actual sizes are rounded up to the nearest grid point.
$ LX_MIN = 15 * L_RMS
$ LY_MIN = 6 * W_0
$ LZ_MIN = LY_MIN
# Grid spacings
$ DX = WAVELENGTH / N_LAMBDA_X
```

```
$ DY = WAVELENGTH / N_LAMBDA_T
$ DZ = DY
# Global grid size
$ NX = int(math.ceil(LX_MIN / DX))
$ NY = 2 * int(math.ceil(LY_MIN / (2 * DY)))
$ NZ = 2 * int(math.ceil(LZ_MIN / (2 * DZ)))
# Add the PML
$ NY_PML = NPML
$ NZ_PML = NPML
# Total grid sizes and intermediate indices
$ NY_BEGIN = NY_PML
$ NY_END = NY_BEGIN + NY
$ NY_TOT = NY_END + NY_PML
$ NZ_BEGIN = NZ_PML
$ NZ_END = NZ_BEGIN + NZ
$ NZ_TOT = NZ_END + NZ_PML
# Global domain sizes
$ LX = NX * DX
$ LY_TOT = NY_TOT * DY
$ LZ_TOT = NZ_TOT * DZ
# Lower coordinate bounds.  The x-coordinate can start at zero, since we'll launch the laser pulse right at
the start of the plasma ramp.
$ XSTART = 0.
$ YSTART = -0.5 * LY_TOT
$ ZSTART = -0.5 * LZ_TOT
# Intermediate coordinates
$ LY_BEGIN = YSTART + NY_BEGIN * DY
$ LY_END = YSTART + NY_END * DY
$ LZ_BEGIN = ZSTART + NZ_BEGIN * DZ
$ LZ_END = ZSTART + NZ_END * DZ
# Additional indices for input block convenience
$ NX1 = NX + 1
$ NY_TOT1 = NY_TOT + 1
$ NZ_TOT1 = NZ_TOT + 1
$ NXm1 = NX - 1
$ NY_TOTm1 = NY_TOT - 1
$ NZ_TOTm1 = NZ_TOT - 1
# Inverse grid spacings
$ DXI = 1 / DX
$ if NDIM >= 2
$ DYI = 1 / DY
$ else
$ DYI = 0.
$ endif
$ if NDIM >= 3
$ DZI = 1 / DZ
$ else
$ DZI = 0.
$ endif
# Courant condition
$ DL = 1 / math.sqrt(DXI*DXI + DYI*DYI + DZI*DZI)
```

```
$ DT = CDTFAC * DL / LIGHTSPEED
# ---------------------------------------------------------------------
# Particles per cell
$ if NDIM == 1
$ PPCX = PPCX_1
$ PPCY = 1.
$ PPCZ = 1.
$ endif
$ if NDIM == 2
$ PPCX = PPCX_2
$ PPCY = PPCY_2
$ PPCZ = 1.
$ endif

$ if NDIM == 3
$ PPCX = PPCX_3
$ PPCY = PPCY_3
$ PPCZ = PPCZ_3
$ endif
$ PPC = PPCX * PPCY * PPCZ
#---------------------------------------------------------------------
# Plasma loading parameters
# Keep the particles away from the PML.
$ MAXRADIUS = 0.95 * LY_END
$ NOMDENS = DENSITY
$ YSTART_LOAD = max(-MAXRADIUS, LY_BEGIN)
$ ZSTART_LOAD = max(-MAXRADIUS, LZ_BEGIN)
$ YEND_LOAD   = min(MAXRADIUS, LY_END)
$ ZEND_LOAD   = min(MAXRADIUS, LZ_END)
# ---------------------------------------------------------------------
# PML parameters
$ SIGMA_OPT = 0.8 * (PML_EXP + 1) * LIGHTSPEED / DY
$ SIGMA_MAX = SIGMA_FAC * SIGMA_OPT
# ---------------------------------------------------------------------
# Run parameters
# Start shifting as soon as the front of the truncated pulse nearly reaches the right edge
$ SHIFTPOS = LX - 0.5 * L_RMS
# Run for 10% longer than the plasma length
$ SIMLENGTH = 1.1 * ENDPLASMA
$ SIMTIME = SIMLENGTH / LIGHTSPEED
# Dump a fixed number of times
$ NDUMPS = 50
$ DUMPTIME = SIMTIME / NDUMPS
$ DUMP_PER = int(math.ceil(DUMPTIME / DT))
$ NSTEPS = NDUMPS * DUMP_PER
##########################################################################
# VORPAL input blocks
##########################################################################
# The following two variables determine the basic object
dimension = NDIM
floattype = double
```

```
# time step, number of steps, etc.
dt = DT
nsteps = NSTEPS
dumpPeriodicity = DUMP_PER
# The grid
<Grid globalGrid>
  numCells   = [NX NY_TOT NZ_TOT]
  lengths = [LX LY_TOT LZ_TOT]
  startPositions = [XSTART YSTART  ZSTART]
  maxIntDepHalfWidth = 2
</Grid>
# The decomposition (determines periodicity)
<Decomp decomp>
  decompType = regular
</Decomp>
# Moving window
downShiftDir = 0
downShiftPos = SHIFTPOS
#=========================================================================
# PIC electromagnetic fields
#=========================================================================
<EmField myEmField>
  kind = yeeEmField

# Boundary condition for launching the laser pulse, polarized in the z- direction
  <BoundaryCondition pumpLauncher>
    kind = variable
    minDim = 1
    lowerBounds = [0  NY_BEGIN  NZ_BEGIN]
    upperBounds = [1  NY_END    NZ_END  ]
    components = [2]
    <STFunc component2>
      kind = gaussianPulse
      omega = OMEGA
      k = [K_0  0.  0.]
      vg = LIGHTSPEED
      L_fwhm = L_FWHM
      widths = [L_HALF  WYPUMP  WZPUMP]
      amplitude = E_0
      phase = 0.
      origin = [XSTARTPUMP  0.0  0.0]
      waistDisplacement = WAISTPOS
    </STFunc>
  </BoundaryCondition>

  <BoundaryCondition rightConductor>
    lowerBounds = [NX       -1       -1]
    upperBounds = [NX1  NY_TOT1  NZ_TOT1]
    minDim      = 2
    kind        = constant
    components     = [1  2 ]   # Ey and Ez
```

```
  amplitudes  = [0. 0.]
 </BoundaryCondition>

 <BoundaryCondition backConductor>
  lowerBounds = [ -1   0       -1]
  upperBounds = [NX1   1   NZ_TOT1]
  minDim      = 2
  kind        = constant
  components     = [0  2 ]   # Ex and Ez
  amplitudes  = [0. 0.]
 </BoundaryCondition>

 <BoundaryCondition frontConductor>
  lowerBounds = [ -1   NY_TOT        -1]
  upperBounds = [NX1   NY_TOT1   NZ_TOT1]
  minDim      = 2
  kind        = constant
  components     = [0  2 ]   # Ex and Ez
  amplitudes  = [0. 0.]
 </BoundaryCondition>

 <BoundaryCondition bottomConductor>
  lowerBounds = [ -1       -1   0]
  upperBounds = [NX1  NY_TOT1   1]
  minDim      = 3
  kind        = constant
  components     = [0  1 ]   # Ex and Ey
  amplitudes  = [0. 0.]
 </BoundaryCondition>

 <BoundaryCondition topConductor>
  lowerBounds = [ -1       -1   NZ_TOT ]
  upperBounds = [NX1  NY_TOT1   NZ_TOT1]
  minDim      = 3
  kind        = constant
  components     = [0  1 ]   # Ex and Ey
  amplitudes  = [0. 0.]
 </BoundaryCondition>
# ----------------------------------------------------------------------
# PML
 <UpdateRegion>
  lowerBounds = [ 0   NY_BEGIN   NZ_BEGIN]
  upperBounds = [NX   NY_END     NZ_END  ]
 </UpdateRegion>

 <PmlRegion Pml>
  energyWritePeriod  = 1000
  eFieldName         = YeeElecField
  bFieldName         = YeeMagField
  ampereUpdaterName  = yeeAmpere
  faradayUpdaterName = yeeFaraday
```

```
# region inside PML (corresponds to Maxwell update region)
   <Region inner>
     lowerBounds = [ 0   NY_BEGIN   NZ_BEGIN]
     upperBounds = [NX   NY_END     NZ_END  ]
   </Region>

# outer bounds of PML
   <Region outer>
     lowerBounds = [ 0       0       0]
     upperBounds = [NX   NY_TOT   NZ_TOT]
   </Region>

# functional form for conductivity
   sigmaForm = SIGMA_MAX * abs(w)^PML_EXP
  </PmlRegion>
</EmField>
#=====================================================================
# Cold, quiet PIC electrons (plasma)
#=====================================================================
<Species plasmaElectrons>
  kind = relBorisVWTagged
  charge = ELECCHARGE
  mass = ELECMASS
  emField = myEmField

# Nominal density and particles per cell at that density
  nominalDensity = NOMDENS
  nomPtclsPerCell = PPC

# Insure the tags are generated by the species so they will restore
  overwriteTag = true
# ---------------------------------------------------------------
# Particle source for the plasma channel
# ---------------------------------------------------------------
  <ParticleSource rampSrc>
    kind = xvLoaderEmitter
# This determines the interval of times for emission and loading, with loading subject to the flags below.
    applyTimes = [0. 1.]
# The following variable determines whether particles are loaded into the new row for a moving window.
    loadOnShift = true
# The following variable determines whether one continues to load with each new time step.
    loadAfterInit = false
# The following determines how positions are defined.  This is the NEW GRID LOADER...
    <PositionGenerator gridSlab>
      kind = gridPosGen
# The following gives the slab over which particles are loaded.  If it is not present or has zero volume, no
particles are loaded.
      <Slab loadSlab>
        lowerBounds = [0.0 YSTART_LOAD ZSTART_LOAD]
        upperBounds = [ 1. YEND_LOAD   ZEND_LOAD]
```

```
    </Slab>
# The following (must be an integer) determines the sign of the normal (For some reason, this must be present, even though we are not emitting)
    emitSign = 1
# The following gives the number of macroparticles loaded per each direction in a cell (on average for varying grids).  So the number per cell is the product of those below.
    macroPerDir = [PPCX PPCY PPCZ]
   </PositionGenerator>
# The following determines how velocities are chosen for loading.  The 'funcVelGen' velocity generator sets the value of the velocity components according to a user-specified space-time function.  In this example, only component 3 is specified--which corresponds to the particle weight--and the other components (0,1,2) default to 0 everywhere.
   <VelocityGenerator rampVelGen>
    kind = funcVelGen
    <STFunc component3>
        kind = tagGen
    </STFunc>

    <STFunc component4>
     kind = cosineFlattop
     direction = [1. 0. 0.]
     startPosition = STARTRAMP
     startFlattop  = STARTFLAT
     endFlattop    = ENDFLAT
     endPosition   = ENDPLASMA
     startAmplitude = 0.0
     flattopAmplitude = 1.
     endAmplitude   = 0.0
    </STFunc>

   </VelocityGenerator>
  </ParticleSource>

# Particle sinks at the simulation boundaries
# ------------------------------------------------------------------------
  <ParticleSink leftAbsorber>
   kind = absorber
   minDim = 1
   lowerBounds = [-1       -1       -1]
   upperBounds = [ 0  NY_TOT1  NZ_TOT1]
  </ParticleSink>

  <ParticleSink rightAbsorber>
   kind = absorber
   minDim = 1
   lowerBounds = [NX       -1       -1]
   upperBounds = [NX1  NY_TOT1  NZ_TOT1]
  </ParticleSink>

  <ParticleSink frontAbsorber>
   kind = absorber
```

```
  minDim = 2
  lowerBounds = [ 0  -1       -1]
  upperBounds = [NX   0  NZ_TOT1]
 </ParticleSink>

 <ParticleSink backAbsorber>
  kind = absorber
  minDim = 2
  lowerBounds = [ 0  NY_TOT        -1]
  upperBounds = [NX  NY_TOT1  NZ_TOT1]
 </ParticleSink>

 <ParticleSink bottomAbsorber>
  kind = absorber
  minDim = 3
  lowerBounds = [ 0       0  -1]
  upperBounds = [NX  NY_TOT   0]
 </ParticleSink>

 <ParticleSink topAbsorber>
  kind = absorber
  minDim = 3
  lowerBounds = [ 0       0  NZ_TOT ]
  upperBounds = [NX  NY_TOT  NZ_TOT1]
 </ParticleSink>

</Species>
# ======================================================================
# History to track particles that obtain high energy
# ======================================================================
<History trajectory>
 kind = speciesTrackTag
 xComponents = all

# List of tags to be tracked: in a file - as integers. tagsFromFile=lwfaTags_tags.txt OR manually in an
array
 tags = [617281  554475  547083  524738  676274  554306  580347  665329 \
    687531  687362  650402  620856  558002  521211  550610  672747  550779 \
    668904 583874  691058  683835  646875]

# OR give a maximum tag to be tracked. Any particle with a tag less than the maximum tag will be
tracked. maximumTag = 4
# OR get the tags from the initial distribution of species can use maximum tag at the same time
getTagsFromSpecies = 1
# species to be tracked
 species = plasmaElectrons

</History>
```

REFERENCES

[1] Tajima, T., and J. M. Dawson, 1979, Phys. Rev. Lett. **43**, 267.

[2] Buneman, O., 1959, Phys. Rev. **115**, 503.

[3] www.txcorp.com

[4] Litvak, A. G., 1969, Zh. Eksp. Teor. Fiz. **57**, 629.

[5] Sprangle, P., C. M. Tang, and E. Esarey, 1987, IEEE Trans. Plasma Sci. **PS-15**, 145

[6] E. Esarey, C. B. Schroeder, and W. P. Leemans Rev. Mod. Phys. **81**, 1229 – Published 27 August 2009

[7] Q. Yu, Y. J. Gu, X. F. Li, S. Huang, Q. Kong, and S. Kawata, Physics of Plasmas **22**, 073107 (2015)

[8] Rosenbluth, M. N., and C. S. Liu, 1972, Phys. Rev. Lett. **29**, 701.

[9] Joshi, C., T. Tajima, J. M. Dawson, H. A. Baldis, and N. A.Ebrahim, 1981, Phys. Rev. Lett. **47**, 1285.

[10] Leemans, W. P., C. W. Siders, E. Esarey, N. E. Andreev, G. Shvets, and W. B. Mori, 1996, IEEE Trans. Plasma Sci. **24**, 331

[11] Dawson, J. M., 1959, Phys. Rev. **113**, 383.

[12] John R. Cary and Allan N. Kaufman, Phys. Fluids **24**, 1238 (1981)

[13] Sprangle, P., E. Esarey, J. Krall, and G. Joyce, 1992, Phys. Rev. Lett. **69**, 2200.

[14] Chen, X. L., and R. N. Sudan, 1993, Phys. Fluids B **5**, 1336.

[15] Esarey, E., P. Sprangle, J. Krall, A. Ting, and G. Joyce, 1993, Phys. Fluids B **5**, 2690.

[16] Gorbunov, L. M., and V. I. Kirsanov, 1987, Sov. Phys. JETP **66**, 290.

[17] Sprangle, P., E. Esarey, A. Ting, and G. Joyce, 1988, Appl. Phys. Lett. **53**, 2146.

[18] Esarey, E., A. Ting, P. Sprangle, and G. Joyce, 1989, Comments Plasma Phys. Controlled Fusion **12**, 191.

[19] Teychenné, D., G. Bonnaud, and J. Bobin, 1993, Phys. Rev. E **48**, R3248.

[20] Sprangle, P., E. Esarey, and A. Ting, 1990a, Phys. Rev. A **41**, 4463.

[21] Sprangle, P., E. Esarey, and A. Ting, 1990b, Phys. Rev. Lett. **64**, 2011

[22] Berezhiani, V. I., and I. G. Murusidze, 1990, Phys. Lett. A **148**, 338.

[23] E. Esarey, C. B. Schroeder and W. P. Leemans, Rev.of Modern Phys. **81** (2009) 1229

[24] Bulanov, S. V., V. I. Kirsanov, and A. S. Sakharov, 1989, JETP Lett. **50**, 198

[25] Akhiezer, A. I., and R. V. Polovin, 1956, Zh. Eksp. Teor. Fiz. **30**, 915 [Sov. Phys. JETP 3, 696 (1956)]

[26] Esarey, E., and M. Pilloff, 1995, Phys. Plasmas **2**, 1432.

[27] Rosenzweig, J. B., 1988, Phys. Rev. A **38**, 3634.

[28] Schroeder, C. B., E. Esarey, B. A. Shadwick, and W. P. Leemans, 2006, Phys. Plasmas **13**, 033103.

[29] Kalmykov, S. Y., L. M. Gorbunov, P. Mora, and G. Shvets, 2006, Phys. Plasmas **13**, 113102

[30] A. Pukhov, J. Meyer-ter-Vehn, Applied Physics B, **Vol 74,** 4-5, pp. 355-361 (2002)

[31] I. Kostyukov, A. Pukhov, S. Kiselev, Physics of Plasmas, **Vol 46**, 12B (2004)

[32] Michel, P., C. B. Schroeder, B. A. Shadwick, E. Esarey, and W. P. Leemans, 2006, Phys. Rev. E **74**, 026501.

[33] I. Kostyukov, E. Nerush, E. Nerush, A. Pukhov, V. Seredov. Physical Review Letters, **Vol. 103,** 17, p.175003 (2009)

[34] A. Pukhov, S. Gordienko Phil. Trans. R. Soc. A, **364**, pp. 623-644 (2006)

[35] S. Gordienko, A. Pukhov, Physics of Plasmas, **12**, 043109 (2005)

[36] Esarey, E., and A. Ting, 1990, Phys. Rev. Lett**. 65**, 1961

[37] Sprangle, P., E. Esarey, and J. Krall, 1996b, Phys. Rev. E **54**, 4211.

[38] Esarey, E., B. A. Shadwick, C. B. Schroeder, and W. P. Leemans, 2004, in *Proceedings of the Advanced Accelerator Concepts Workshop*, edited by V. Yakimenko (AIP, New York), **Vol. 737**, pp. 578–584

[39] Shadwick, B. A., C. B. Schroeder, and E. Esarey, 2009, Phys. Plasmas **16**, 056704.

[40] Teychenné, D., G. Bonnaud, and J.-L. Bobin, 1994b, Phys. Rev. E **49**, 3253

[41] Katsouleas, T., 1986, Phys. Rev. A **33**, 2056

[42] Sprangle, P., B. Hafizi, J. R. Peñano, R. F. Hubbard, A. Ting, C. I. Moore, D. F. Gordon, A. Zigler, D. Kaganovich, and T. M. Antonsen, Jr., 2001, Phys. Rev. E **63**, 056405.

[43] E. Esarey, C. B. Schroeder, and W. P. Leemans, Rev. Mod. Phys. **81**, 1229 – Published 27 August 2009

[44] K. V. Lotov Phys. Plasmas **22**, 103110 (2015)

[45] John M. Dawson Rev. Mod. Phys. **55**, 403 (1983)

[46] O. Buneman Phys. Rev. **115**, 503 (1959)